Available online at www.sciencedirect.com
ScienceDirect
International Journal of Solids and Structures 45 (2008) 1845–1875
INTERNATIONAL JOURNAL OF SOLIDS AND STRUCTURES
www.elsevier.com/locate/ijsolstr

On the microstructure of open-cell foams and its effect on elastic properties

Wen-Yea Jang [a], Andrew M. Kraynik [b], Stelios Kyriakides [a,*]

[a] Research Center for Mechanics of Solids, Structures and Materials, The University of Texas at Austin, WRW 110, Austin, TX 78712, USA
[b] Sandia National Laboratories, Albuquerque, NM, USA

Received 20 July 2007; received in revised form 2 October 2007
Available online 24 October 2007

Abstract

Synthetic open-cell foams have a complex microstructure consisting of an interconnected network of cells resulting from the foaming process. The cells are irregular polyhedra with anywhere from 9 to 17 faces in nearly monodisperse foams. The material is concentrated in the nearly straight ligaments and in the nodes where they intersect. The mechanical properties of such foams are governed by their microstructure and by the properties of the base material. In this study micro-computed X-ray tomography is used to develop 3D images of the morphology of polyester urethane and Duocel aluminum foams with different average cell sizes. The images are used to establish statistically the cell size and ligament length distributions, material distributions along the ligaments, the geometry of the nodes and cell anisotropy. The measurements are then used to build finite element foam models of increasing complexity that are used to estimate the elastic moduli. In the most idealized model the microstructure is represented as a regular Kelvin cell. The most realistic models are based on Surface Evolver simulations of random soap froth with N^3 cells in spatially periodic domains. In all models the cells are elongated in one direction, the ligaments are straight but have a nonuniform cross sectional area distribution and are modeled as shear deformable beams. With this input both the Kelvin cell models and the larger random foam models are shown to predict the elastic moduli with good accuracy but the random foams are 5–10% stiffer.

Keywords: Open-cell foams; Elastic properties; Microstructure

1. Introduction

Synthetic cellular materials such as open-cell foams have a complex microstructure consisting of an interconnected network of ligaments that form along the edges of randomly packed cells that evolve during the foaming process. The cells are irregular polyhedra with anywhere from 9 to 17 faces when the foam is nearly monodisperse (see Fig. 1). The material is concentrated in the nearly straight edges of the polyhedra and in the nodes where they intersect, usually four at a time (Figs. 2 and 3). The design and use of foams require that the

* Corresponding author.
E-mail address: skk@mail.utexas.edu (S. Kyriakides).

0020-7683/$ - see front matter © 2007 Elsevier Ltd. All rights reserved.
doi:10.1016/j.ijsolstr.2007.10.008

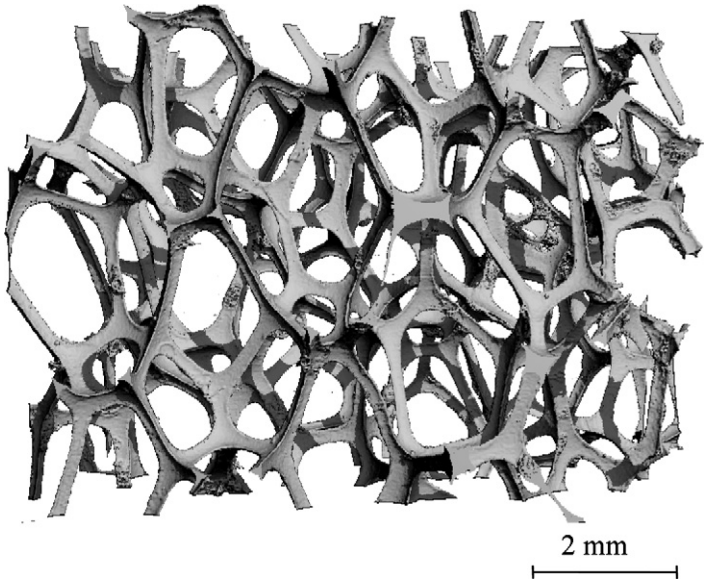

Fig. 1. Computed tomography image of a 20-ppi polyester urethane foam ($\rho^*/\rho = 2.36\%$).

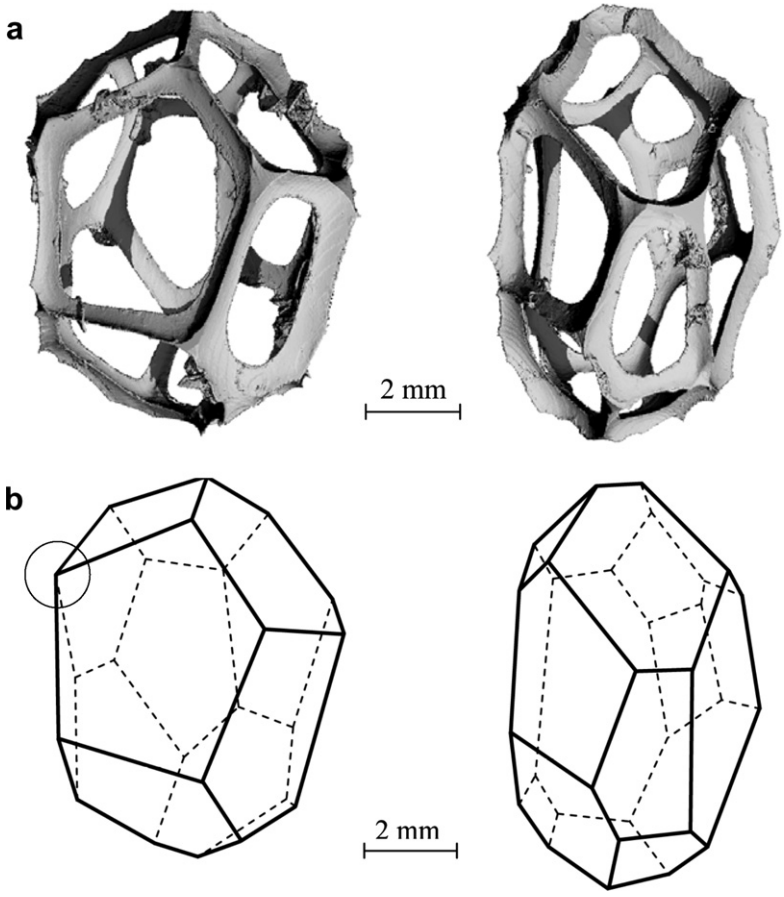

Fig. 2. (a) Cells extracted from a 3-ppi polymeric foam illustrating irregular polyhedral geometry. Polyhedra are somewhat elongated in rise direction. (b) Skeletal drawing of the cells in (a).

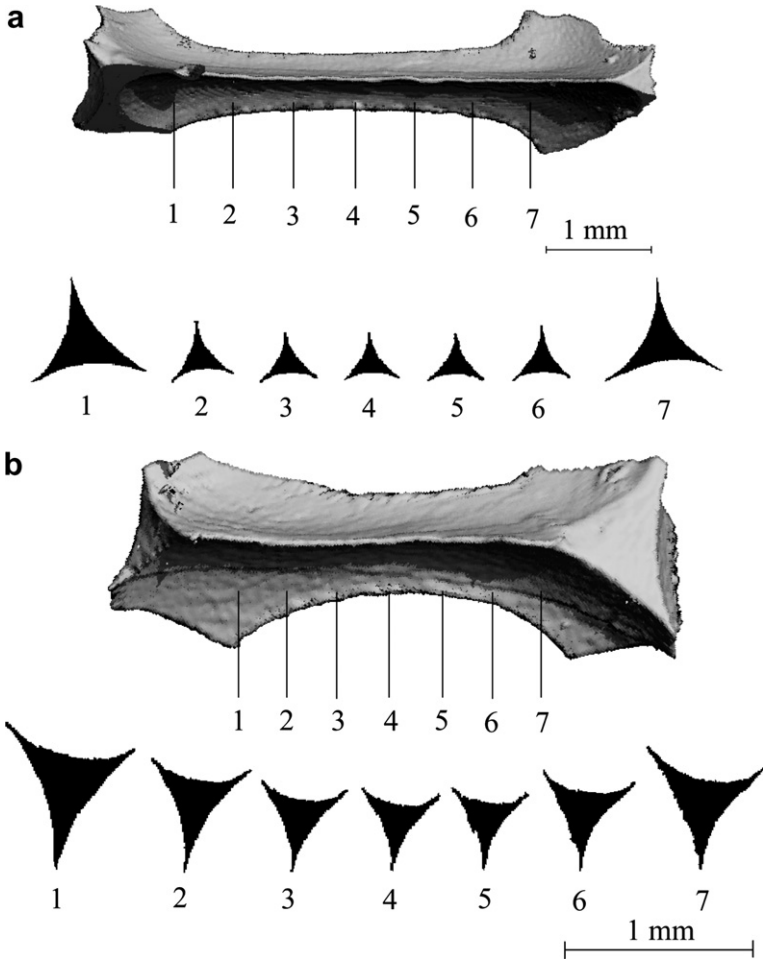

Fig. 3. Ligaments from a 3-ppi foam and cross sectional views: (a) $\ell \approx 4.2$ mm and (b) $\ell \approx 2.1$ mm.

microstructure be related to the properties (mechanical, thermal, acoustical, etc.). Gibson and Ashby's book (1997) gives an excellent review on a broad range of cellular materials, natural and manmade. Hilyard and Cunningham (1994), Weaire and Hutzler (1999), an MRS Bulletin (2003) and the book by Ashby et al. (2000) cover a broad range of foam issues from manufacture to application. Gong et al. (2005) (referred to as GKJ henceforth) presented geometric information about a class of open-cell polyester urethane (PU) foams that included cell and ligament geometry and the distribution of the material in the ligaments and nodes. They then used this information to generate model foams based on the 14-sided cell of Kelvin. It was shown that geometric characteristics such as the material distribution in the ligaments and nodes, and the cell anisotropy play a decisive role in the mechanical behavior of the foams. These characteristics are essential for quantitatively accurate predictions of all mechanical properties (see also Gong and Kyriakides, 2005; Mills, 2007).

The present study builds on the work of GKJ by providing a more systematic and detailed study of the microstructure of the same PU foams by using micro-computed X-ray tomography. Micro-CT generated 3D images are used to establish statistically cell sizes and polyhedra types, ligament length distributions, material distributions along the ligaments and prevalent geometric anisotropies. The same tools are also used to study the microstructure of a class of aluminum (Al) open-cell foams with three different average cell sizes. The measurements are subsequently used to generate a hierarchy of 3D renderings of the microstructure that are increasingly more realistic. The renderings are used in FE models to estimate the elastic properties of the foams. The most idealized model is the Kelvin cell microstructure assigned some of the measured geometric

characteristics in the manner of GKJ. More realistic random microstructures are based on Surface Evolver (Brakke, 1992) simulations of soap froth. A more detailed literature review can be found in GKJ.

2. Morphology of polymeric and aluminum foams

We have analyzed foams with different average cell size and base material: (a) polyester urethane foams of several cell sizes manufactured by Foamex and (b) aluminum (Al-6101-T6) Duocel® foams manufactured by ERG. Computed X-ray tomography was used to characterize the foam microstructure including cell size and distribution, anisotropy, ligament length and area distribution, etc. The measured geometric characteristics will later be used to generate FE models of the foams for calculating their mechanical properties. We start with a brief introduction to X-ray tomography as used in this study.

2.1. Micro-computed X-ray tomography

Computed X-ray tomography is a nondestructive technique for 3D visualization of solid bodies (ASTM E 1441-00 (1992), Ketcham and Carlson (2001)). Gray levels in CT images correspond to the linear attenuation coefficient, which is a function of the density and atomic number of the material being scanned and the X-ray energy. A slice image is taken by first sending a thin fan of X-rays from a point source though the body. As the X-rays pass though the body, they are attenuated differently by regions of different density (e.g., edges of the body, holes, etc.) and the net attenuation along each ray path is recorded by a detector. The signals are stored and a new signal is sent from a slightly different angle. This is repeated N times until images are recorded for a complete revolution. Software is then used to process the N angular images and to reconstruct the 3D attenuation map of the slice. The process is repeated for neighboring slices until the whole body is scanned. The slices are then assembled to form a 3D image of the whole body.

The method is used extensively in medicine where the patient is stationary and the X-ray source and detector rotate around the body. A Micro-CT is a desktop device used for smaller objects (a few centimeters in diameter). Here the source and the detector are stationary while the object rotates. In the present study we employed a *Scanco Medical AG* Micro-CT-80 (μCT 80). Its major characteristics are listed in Appendix A.

2.2. Polyester urethane foam morphology

GKJ used optical and SEM microscope images to analyze five PU *Foamex-SIF* foams with nominal cell sizes of 3, 10, 20, 45 and 100 pores per inch (ppi) and relative densities (ρ^*/ρ) in the range of 2.2–2.8%. The measurements performed included cell size, cell anisotropy and ligament length (Montminy et al. (2004) analyzed polyurethane foams using micro-CT and a custom image processing algorithm, and reported geometric characteristics of a 20-ppi foam). Several individual ligaments were manually extracted and sectioned, from which area distribution along the length was established (see Table 1 of GKJ). The micro-CT and its custom software facilitate 3D imaging of the foams, which in turn enabled a more extensive and systematic analysis of the microstructure that did not involve manual extraction of cells and ligaments. In addition, the laborious microtome sectioning of ligaments was now performed digitally. The images shown here were obtained using a peak energy of 45 kVp, current intensity of 177 μA and the highest resolution of our system (2048×2048 pixels).

Fig. 1 shows a 3D image consisting of a few cells from a 20-ppi foam (vertical corresponds to the rise direction). The cells are seen to be irregular polyhedra with nearly straight edges (ligaments) that have the characteristic three-cusp hypocycloid cross section of *Plateau borders*. The foaming process results in some elongation of the cells in the rise direction that is apparent in the figure. The polyhedral geometry of cells is illustrated in Fig. 2a, which shows two individual cells extracted from the coarsest foam. Fig. 2b shows a skeletal outline of the cells formed by joining the centers of adjacent nodes with straight lines. The one on the LHS has 14 faces that include 3 quadrilaterals, 8 pentagons, 3 hexagons and a total of 35 ligaments. The one on the RHS has 17 faces with 3 quadrilaterals, 7 pentagons, 6 hexagons, 1 heptagon and a total of 45 ligaments. Although four ligaments commonly join at a node, higher connectivity is also possible. For example the node circled in Fig. 2b has a connectivity of 6. More data on the geometry of the cells

Table 1
Geometric parameters of polyester urethane foams analyzed

Foam (ppi)	$\frac{\rho^*}{\rho}$ (%)	$\bar{h}_1$ in. (mm)	$h_1\|_{\text{min-max}}$ in. (mm)	$\frac{\Sigma_{h_1}}{\bar{h}_1}$	λ	$\bar{\ell}$ in. (mm)	$\frac{\Sigma_\ell}{\bar{\ell}}$	$\bar{A}_o \times 10^3$ in.^{2} (mm^2)	$\frac{\Sigma_{A_o}}{\bar{A}_o}$
3	2.18	0.323 (8.20)	0.272–0.412 (6.91–10.46)	0.073	1.423	0.112 (2.845)	0.371	0.120 (0.0771)	0.136
10	2.47	0.233 (5.92)	0.190–0.290 (4.83–7.37)	0.073	1.342	0.085 (2.159)	0.313	0.100 (0.0647)	0.522
20	2.36	0.118 (2.997)	0.101–0.135 (2.565–3.429)	0.058	1.276	0.0398 (1.011)	0.443	0.0623 (0.0402)	0.218
45	2.44	0.0524 (1.331)	0.043–0.0623 (1.09–1.582)	0.068	1.247	0.0159 (0.404)	0.285	0.00457 (0.00295)	0.293
100	2.82	0.0182 (0.462)	0.015–0.0239 (0.38–0.607)	0.074	1.211	0.0067 (0.17)	0.313	–	–

$\rho = 0.0432$ lb/in.^{3} (1196 kg/m^3).

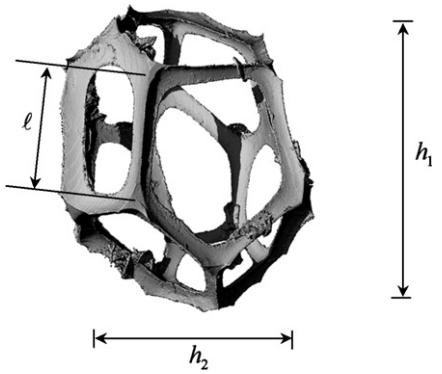

can be found in GKJ who concluded that the geometric characteristics of the cells were quite similar to those reported by Matzke in his classic work (1946) on monodisperse soap froth.

Table 1 summarizes geometric parameters of the five foams of GKJ. The original measurements have been enhanced by new ones performed using micro-CT. Cell size is defined by the average height of the cells in the rise direction $\bar{h}_1$. The range of cell sizes recorded was then used to establish a measure of *polydispersity* based on the ratio of one standard deviation (Σ_{h_1}) and the average cell height $\bar{h}_1$. The results range from 0.074 to 0.058 indicating that cell size variation is small in this type of foam.

The cell diameters in the transverse directions (h_2) was also measured and used to establish the anisotropy parameter $\lambda = h_1/h_2$. The mean values of λ reported in Table 1 vary from about 1.42 to 1.21 and decrease as the cell size decreases. (The values differ slightly from those in GKJ because of additional measurements. Huber and Gibson (1988) reported similar values of anisotropy for a group of polyurethane foams. Montminy et al. (2004) used a more elaborate measure of anisotropy that is an approximation of λ and reported a value of 1.292 for their foam).

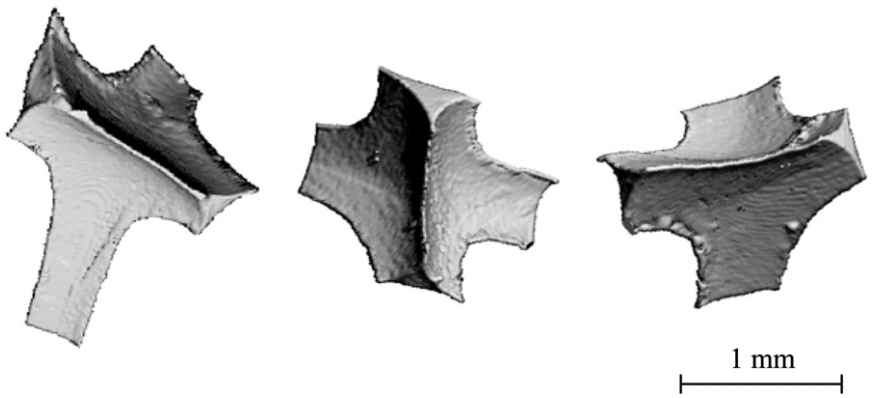

Fig. 4. Images showing three four-ligament nodes from a 3-ppi foam.

Ligament lengths were measured for each foam using micro-CT images. Fig. 3 shows two ligaments of different length extracted from the 3-ppi foam. The length, ℓ, is defined as the distance between the centers of nodes that the ligament connects (center positions are best estimates). The mean value of the measurements is listed under $\bar{\ell}$ while $\Sigma_\ell/\bar{\ell}$ is one standard deviation divided by the mean value. The measurements from all foams were used to generate the frequency (N) vs. length ($\ell/\bar{\ell}$) bar graph shown in Fig. 5. No discernible difference was observed among the five foams.

Fig. 3 shows that the cross sectional area of the ligaments changes along the length. GKJ conducted a limited number of measurements of the area distribution and demonstrated that this is an important parameter for mechanical properties. Similar measurements have been performed by digitally slicing ligaments from two of the foams in the manner shown in Fig. 3. The area of the slices was then determined as a function of axial position. The cross sections have the characteristic Plateau border shape. The area is nearly constant over the central half of the length but increases significantly as the nodes on either end are approached. Fig. 6 shows a plot of the measured cross sectional area $A(\xi)$ normalized by the value at mid-span, A_o, as a function of axial position, $\xi = x/\ell$(included are data from GKJ enriched with new measurements). The data were fitted with the following symmetric function:

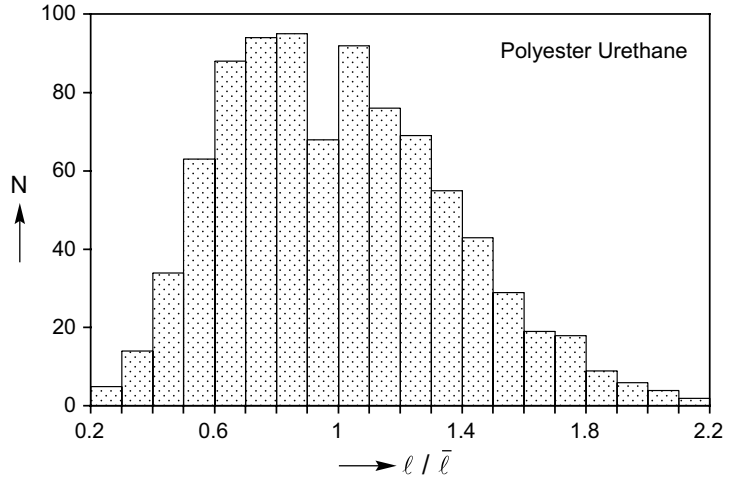

Fig. 5. Plot of frequency vs. normalized length for polyester urethane foams.

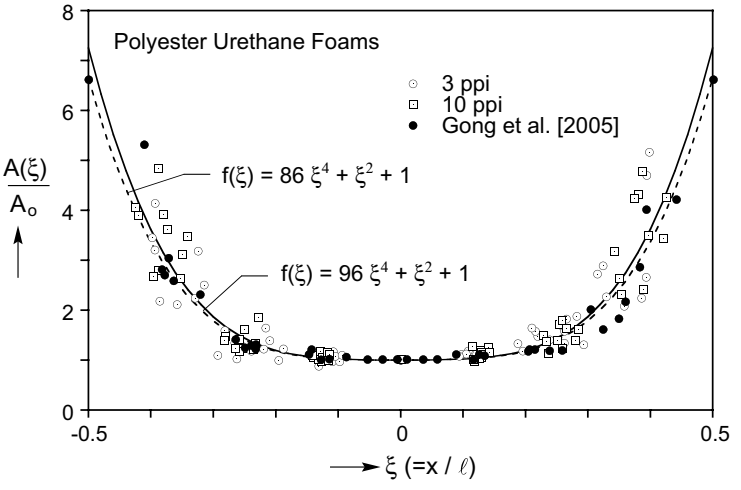

Fig. 6. Measured variation of ligament cross sectional area along the length for PU foams fitted with function $f(\xi)$.

$$A(\xi) = A_o f(\xi) = A_o(c_1\xi^4 + c_2\xi^2 + 1). \quad (1)$$

The constants $c_1 = 96$ and $c_2 = 1$ were found to yield the fit drawn in solid line in Fig. 6. The slightly different fit of GKJ is also included (dashed line) for comparison. In their work GKJ assumed the area at mid-span, A_o, to be a constant. The recent micro-CT measurements showed that longer ligaments tend to have smaller A_o than shorter ones. Measured values of A_o are plotted against ligament length in Fig. 7. Each variable is normalized by the mean value of all the measurements ($\overline{A}_o$ and $\bar{\ell}$ given in Table 1). The following function was generated by fitting the data:

$$A_o(\eta) = \overline{A}_o g(\eta) = \overline{A}_o(d_1 + d_2\eta^{-\beta}), \quad \eta = \ell/\bar{\ell} \quad (2)$$

with $d_1 = 0.5656$, $d_2 = 0.3869$ and $\beta = 1.4297$.

The nodes are zones of material concentration that must be accounted for. Fig. 4 shows images of three isolated nodes from the 3-ppi foam. They are all junctions of four ligaments, which is by far the most commonly occurring type. The nodes are seen to have smooth curved surfaces while simultaneously they are significant concentrations of material. Spatial modeling of the nodes will be addressed in Section 4.3.

2.3. Aluminum (Duocel) foam morphology

Three Al-6101-T6 Duocel open-cell foams made by ERG were analyzed using micro-CT in a similar fashion as the PU foams. The foams were supplied in 4 in. (102 mm) thick blocks with planar dimensions of 12×14.5 in. (305×368 mm). The foams had nominal cell sizes of 10, 20 and 40-ppi and their average relative densities were, respectively, 8.23%, 7.50% and 7.54% (see Table 2). The specimens typically had a 2 in. cross section (51 mm) and either the full or half height of the block. They were removed from the block by using a wire-cut electrical discharge machining (EDM) process to minimize distortion of the cut edges. A small variation in density was observed in the blocks and consequently densities of individual specimens analyzed and/or tested may vary to some degree from the average values listed in Table 2.

Duocel foam is thought to be made by using polymeric foams as templates to generate a mold in which aluminum alloy is cast. On solidification, the mold material is removed leaving behind a replica of the original polymeric foam (Section 2.5, Ashby et al., 2000; see also Zhou et al., 2005). By selecting the template foam it is possible to retain characteristics such as cell size uniformity exhibited by some commercially available polymeric foams. The images that will be presented were obtained using a peak energy of 70 kVp, current intensity of 114 μA and the highest resolution of our system 2048×2048 pixels.

Fig. 8 shows a 3D image of a 10-ppi foam. The main characteristics of the cells are similar to those of the polymeric foam shown in Fig. 1. The polyhedral cells are somewhat elongated in one direction (vertical) but

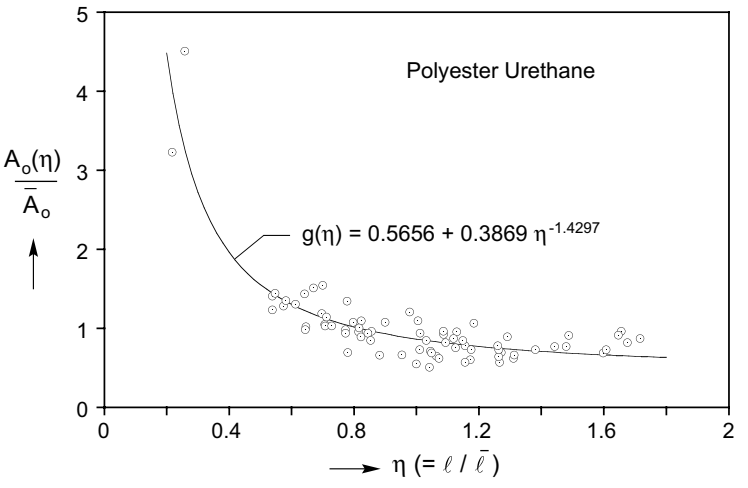

Fig. 7. Measured mid-span cross sectional area as a function of normalized ligament length fitted with function $g(\eta)$ for PU foams.

Table 2
Geometric parameters of Al-6101-T6 foams analyzed

Foam (ppi)	$\frac{\rho^*}{\rho}$ (%)	$\overline{h}_1$ in. (mm)	$h_1\|_{\text{min-max}}$ in. (mm)	$\frac{\Sigma_{h_1}}{\overline{h}_1}$	λ	$\overline{\ell}$ in. (mm)	$\frac{\Sigma_\ell}{\overline{\ell}}$	$\overline{A}_o \times 10^3$ in.^{2} (mm^2)	$\frac{\Sigma_{A_o}}{\overline{A}_o}$
10	8.23	0.184 (4.683)	0.158–0.234 (4.013–5.944)	0.0754	1.27	0.070 (1.780)	0.263	0.459 (0.296)	0.261
20	7.50	0.141 (3.570)	0.120–0.170 (3.048–4.318)	0.0707	1.24	0.048 (1.22)	0.277	0.144 (0.0929)	0.235
40	7.54	0.115 (2.929)	0.087–0.136 (2.210–3.454)	0.0749	1.18	0.041 (1.04)	0.268	0.0648 (0.0418)	0.238

$\rho = 0.0972$ lb/in.^{3} (2690 kg/m^3).

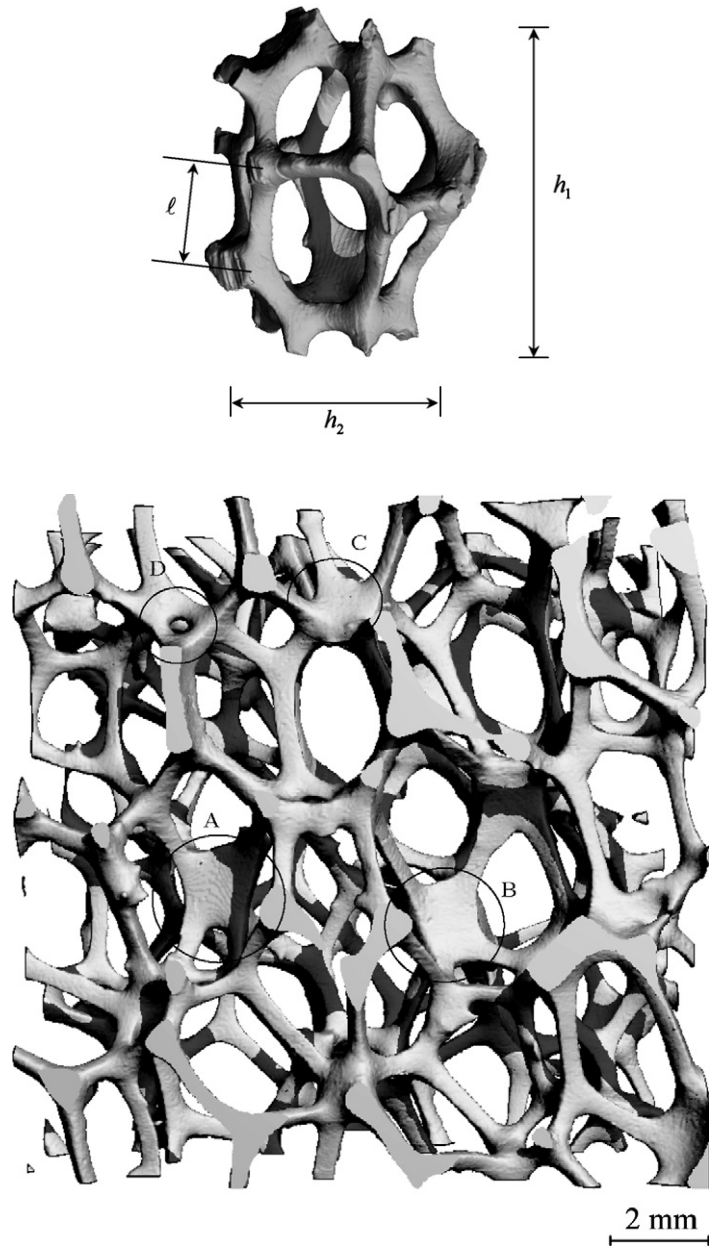

Fig. 8. Computed tomography image of a 10-ppi Al foam ($\rho^*/\rho = 8.23\%$). Four closed faces are circled.

the ligaments have rounder cross sectional profiles. The same features can be seen in Fig. 9a, which shows images of an individual cell and a pair of cells extracted from the same foam. Fig. 9b shows a skeletal outline

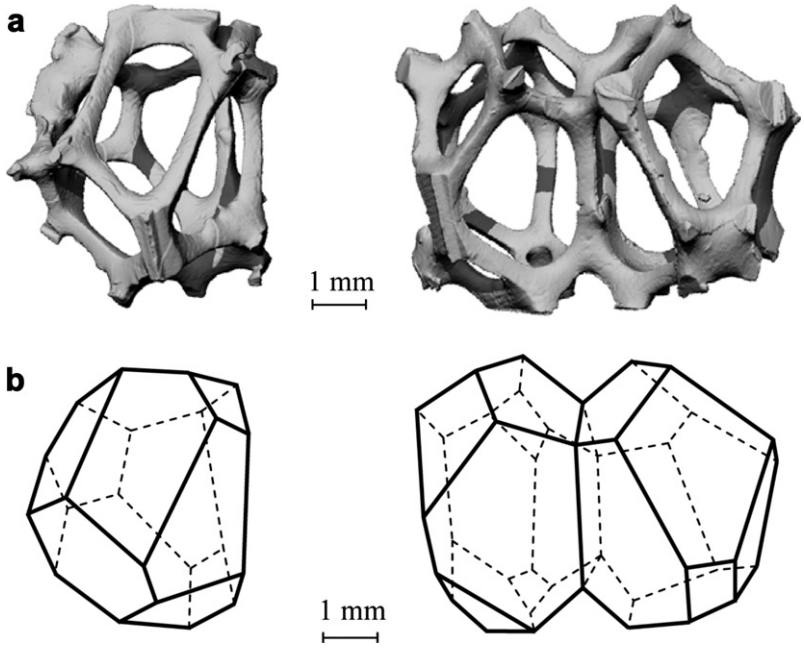

Fig. 9. (a) Cells extracted from a 10-ppi Al foam illustrating irregular polyhedral geometry. (b) Skeletal drawing of the cells in (a).

of the cells formed by joining the centers of adjacent nodes with straight lines. The individual cell in Fig. 9 has 13 faces that include 3 quadrilaterals, 6 pentagons, 4 hexagons and a total of 33 ligaments. In the pair of cells, the one on the LHS has 14 faces with 4 quadrilaterals, 5 pentagons, 5 hexagons and a total of 36 ligaments while the one on the RHS has 12 faces with 2 quadrilaterals, 8 pentagons, 2 hexagons and a total of 30 ligaments. The foams are also anisotropic with anisotropies (see Table 2) that are comparable to those of the PU foams (Benouali et al. (2005) reported anisotropy measurements in closed-cell Al foams).

The average ligament lengths ($\bar{\ell}$) and normalized standard deviations ($\Sigma_\ell/\bar{\ell}$) are listed in Table 2. The distribution of lengths from the three foams is given in the form of a frequency bar graph in Fig. 10. The distribution is similar to the one for the PU foams with a bit more concentration around the mean value. Once again, no significant difference was observed between the distributions of the three foams.

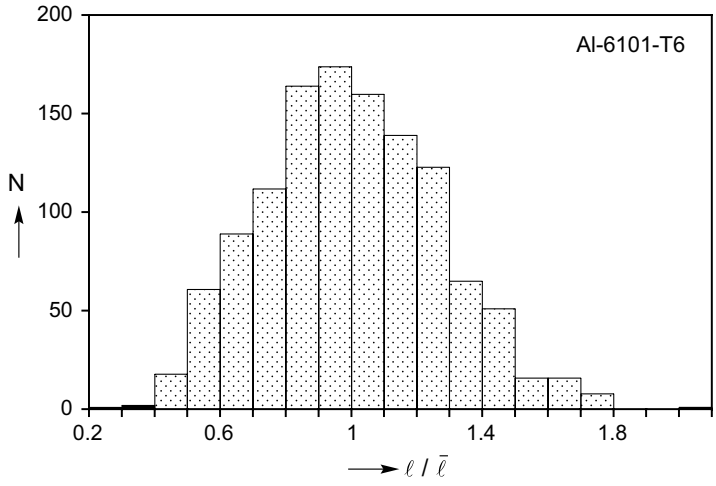

Fig. 10. Plot of frequency vs. normalized length for Al foams.

Fig. 11 shows images of two ligaments from the 10-ppi foam and sets of seven cross sectional images taken along their lengths. The Plateau border shape that must have existed in the polymeric foam templates have been replaced by rounded extrados. The ligaments are overall much bulkier as can be seen by comparing the mean values of the mid-span cross sectional areas ($\overline{A}_o$) listed in Table 2 with the values of the corresponding PU foams in Table 1. The overall heavier microstructure is also supported by the images of three nodes shown in Fig. 12. They are again junctions of four ligaments but the concave shapes of Fig. 4 have been filled in resulting in convex cross sections. These differences are almost certainly caused by the molding process. The net result of the bulkier construction of the ligaments and nodes is that the Al foams contain much more solid than their PU counterparts causing the relative density to increase by a factor of about 3.

One more complicating factor was observed from the micro-CT images. Several sites where relatively small faces such as quadrilaterals presumably existed in the original polymeric template were filled in during the molding process. Four such examples have been circled in Fig. 8 and are identified by letters A–D. All of them appear to have been initially quadrilaterals; cases A–C have closed, while face D has been built up but a small circular hole remains in the middle of the face.

More examples of closed faces can be seen in the three isolated cells included in Fig. 13. The one on the LHS has three closed quadrilaterals. The one in the center has a closed pentagon and the one of the RHS has two closed quadrilaterals. Clearly, such filled-in faces are sites of local material concentration that result

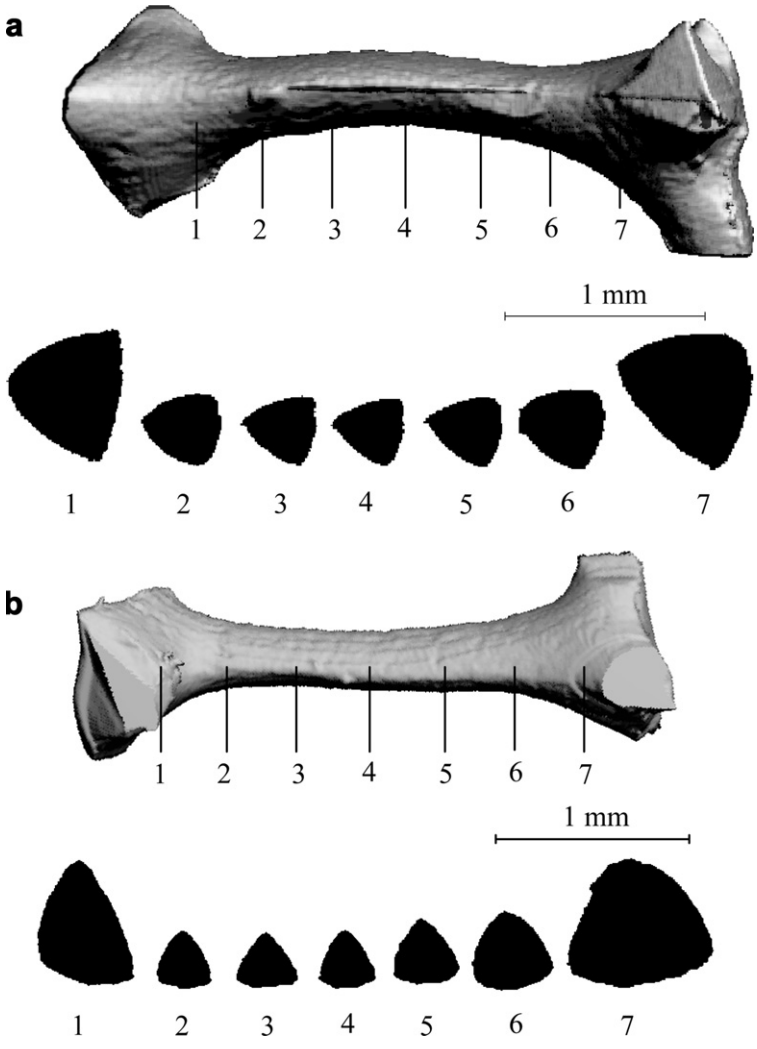

Fig. 11. Ligaments from a 10-ppi Al foam and cross sectional views: (a) $\ell \approx 2.6$ mm and (b) $\ell \approx 2.4$ mm.

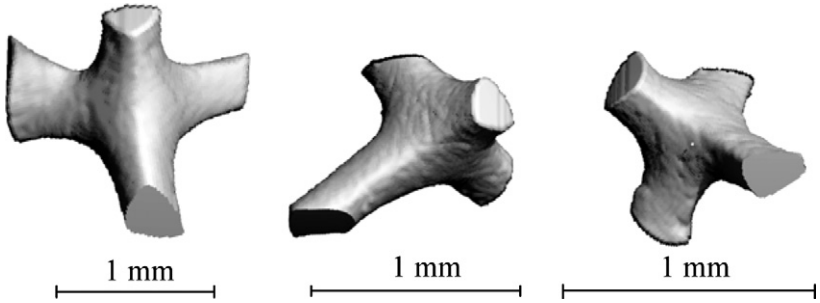

Fig. 12. Images showing three four-ligament nodes from a 10-ppi Al foam.

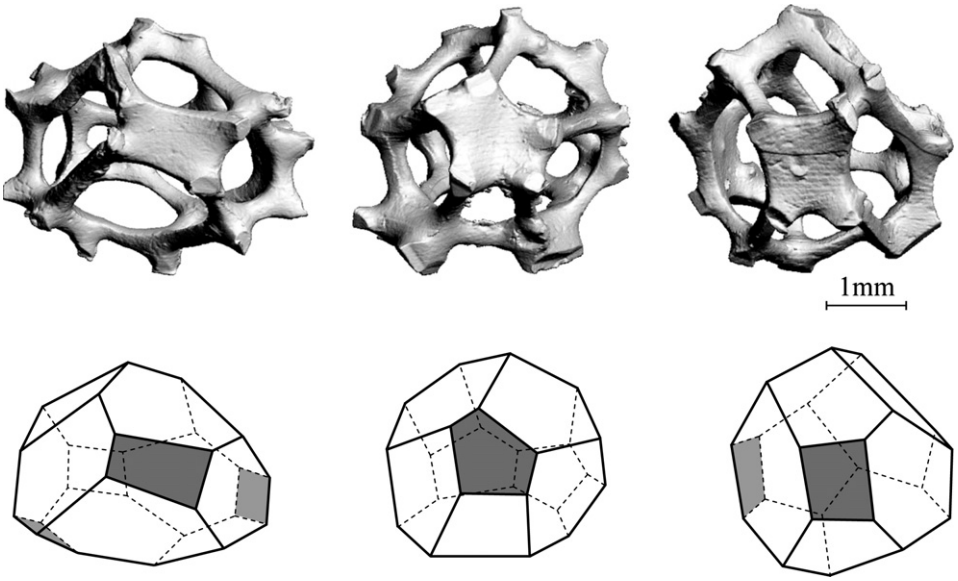

Fig. 13. (a) Three individual cells from a 10-ppi Al foam exhibiting closed faces. (b) Skeletal drawings of the cells with the closed faces shaded.

in local stiffening but more importantly contribute to the overall weight of the foam. We have estimated that the number of closed faces in our foams is on the order of 1 in 20, which is a significant number. We note that such concentrations of material are difficult to account for in periodic models and some consequences of this will be discussed in the analysis section.

Ligament slicing was performed for each of the three Al foams analyzed and two sample slice sets are shown in Fig. 11. The areas of the slices were measured digitally and were used to generate the $A(\xi)/A_o$ vs. ξ plot shown in Fig. 14. The data were then fitted with Eq. (1) yielding $c_1 = 36$ and $c_2 = 1$. Similar to the PU foams, A_o was found to vary with length in the manner shown in Fig. 15. (The normalizing values $\overline{A}_o$ and $\bar{\ell}$ of each and their standard deviations are listed in Table 2.) The measurements were fitted with Eq. (2) yielding the fit parameters $d_1 = 0.6633$, $d_2 = 0.2648$ and $\beta = 2.5963$.

Finally the stress–strain response of the Al-6101-T6 material was measured in a uniaxial test on a 0.48 in. (12.2 mm) diameter solid rod that was cast together with the foam by ERG. The elastic modulus measured was 10^4 ksi (69 GPa).

3. Numerical generation of random foam

A third type of foam model was based on the microstructure of random spatially periodic soap froth simulated with Brakke's Surface Evolver (1992). Up to 1728 equal-volume bubbles are packed in a unit cell (Kray-

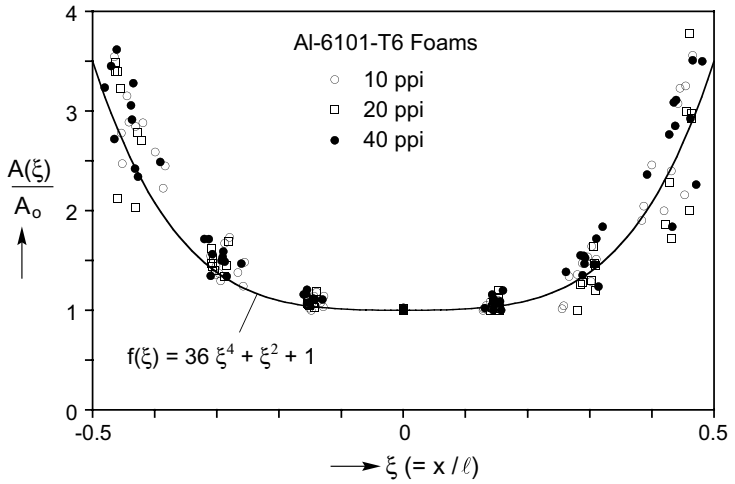

Fig. 14. Measured variation of ligament cross sectional area along the length for Al foams fitted with function $f(\xi)$.

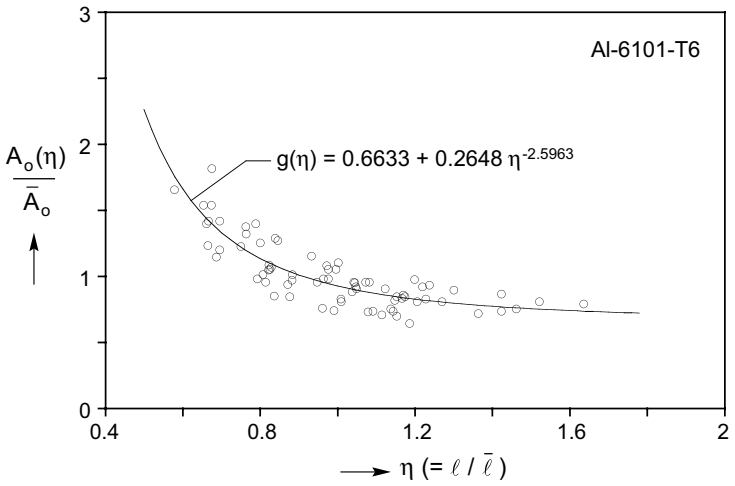

Fig. 15. Measured mid-span cross sectional area as a function of normalized ligament length fitted with function $g(\eta)$ for Al foams.

nik et al., 2003). The geometric characteristics of model soap froth are compared with the solid foams presented in Section 2. The foam skeleton is then used as a template to generate FE models in which the ligaments are represented as space beams. These models are then used to study parametrically the elastic moduli, which are compared with similar results for two idealized microstructures.

The Surface Evolver is the standard software for calculating the equilibrium microstructure of soap froth. A primitive Voronoi froth with foam-like characteristics is first generated from randomly packed hard spheres of equal radius using molecular dynamics. Each Voronoi cell consists of all points that lie closest to a random seed, i.e., the center of each sphere. The Voronoi structure is then used as an initial condition in the Surface Evolver to generate the limiting case of a "dry" foam in which the liquid volume fraction is zero and the films can be modeled as two-dimensional surfaces. The software minimizes energy and balances mechanical forces by satisfying Plateau's laws (Plateau, 1873; Weaire and Hutzler, 1999): I. *the faces of cells are surfaces of constant mean curvature*; II. *three faces meet at equal dihedral angles of 120°*; and III. *four edges meet at the tetrahedral angle* $\cos^{-1}(-1/3) \approx 109.47°$. For monodisperse foam the additional constraint that all cells have the same volume is also applied. The relaxation process requires a large number of topological transitions that involve cell-neighbor switching. Since the solution is a local energy minimum, the surface area can be further

reduced by subjecting the foam to large-deformation tension–compression cycles that provoke additional neighbor switching; this process is referred to as annealing. The resulting structures are in excellent agreement with Matzke's experimental study (1946) of monodisperse soap froth indicating that the foam structures being produced are realistic. The simulations provide accurate data on geometric properties such as the volume, surface area, and edge length of the entire foam, individual cells, and cell-level features (Kraynik et al., 2003a, 2003b, 2004, 2005, 2006).

"Wet" foams of finite density are generated from dry foams through a second step in the Surface Evolver that assumes that all liquid is located in the Plateau borders, an assumption appropriate for open-cell foams. Initially, all edges of the dry foam are "dressed" with liquid prisms of triangular cross section that approximate the target foam density. The Surface Evolver minimizes the surface energy, which shapes the liquid into Plateau borders as shown in Fig. 16. In the process the basic cell geometry evolves to some degree and Plateau's laws do not apply. The calculations demand much more computational effort than dry foams because of the large number of facets required to discretize the Plateau borders (Brakke, 1992).

The foam image shown in Fig. 16 represents a section of a random wet foam with 64 cells and relative density 0.025. The ligaments have Plateau border cross sections with areas that vary along their length. The ligaments as well as the nodes have the same general characteristics as the PU foams shown in Fig. 1. The main difference is that the Surface Evolver generated foam is nearly isotropic. Fig. 17a shows a pair of cells extracted from the same foam and Fig. 17b shows their skeletal version formed by joining the centers of the nodes with straight lines. The two cells have a total of 64 ligaments that form 2 quadrilaterals, 20 pentagons and 5 hexagons.

The fully periodic domain of a particular random wet foam with 512 cells has 6020 ligaments with the distribution of lengths shown in the frequency plot in Fig. 18. The distribution is similar to that of the Al foams in Fig. 10 but is somewhat different from that of the PU foams in Fig. 4. The ligament mid-span cross sectional area varies in the manner shown in Fig. 19. The figure includes corresponding results from the measurements performed on the PU and Al foams. The trend of the present results is seen to follow that of the measurements quite well.

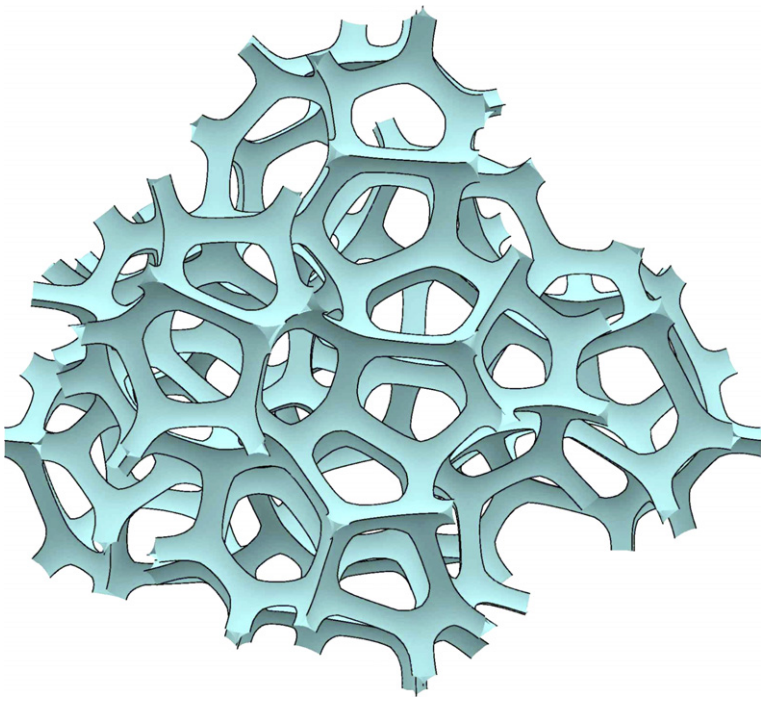

Fig. 16. Image of an isotropic random foam generated by Surface Evolver ($\rho^*/\rho = 2.5\%$).

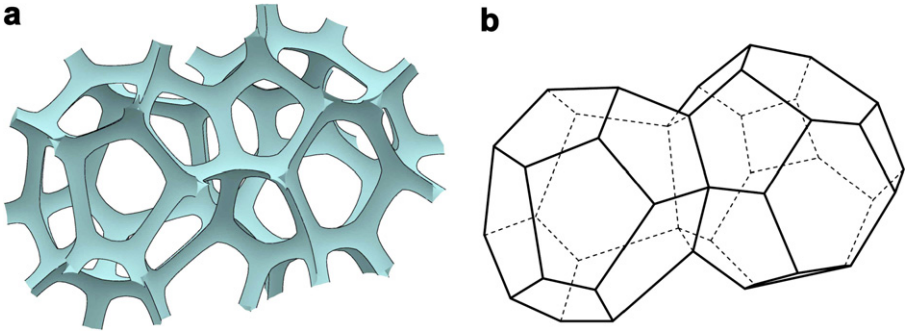

Fig. 17. (a) Cells extracted from the random foam shown in Fig. 16. (b) Skeletal drawing of the cells in (a).

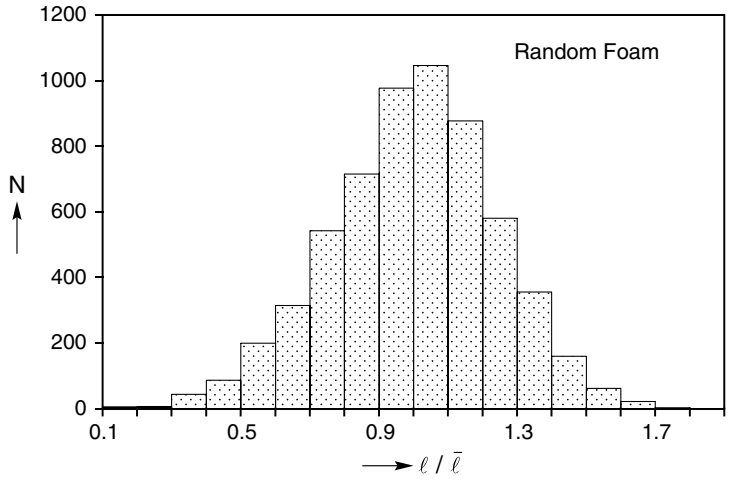

Fig. 18. Plot of frequency vs. normalized length for random foam model.

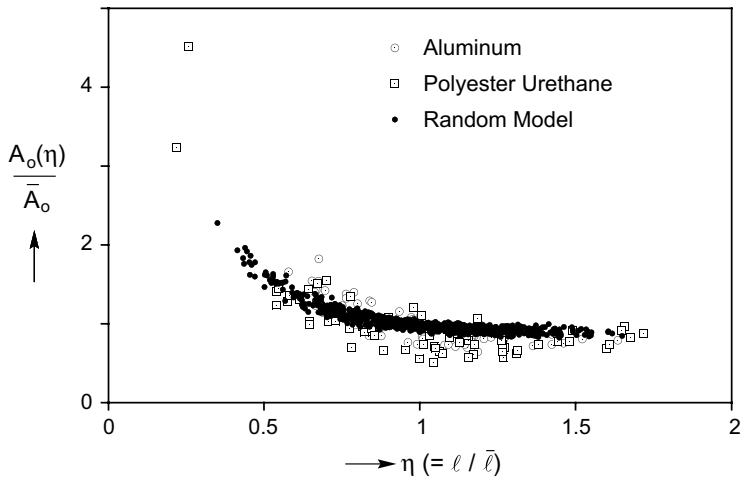

Fig. 19. Normalized mid-span cross sectional area versus normalized ligament length of random foam model, the PU and Al foams.

The random foam model that will be used in the subsequent calculations is based on the dry foam precursor of the wet foam with 512 cells. Assigning geometric characteristics to the ligaments is discussed in the next section.

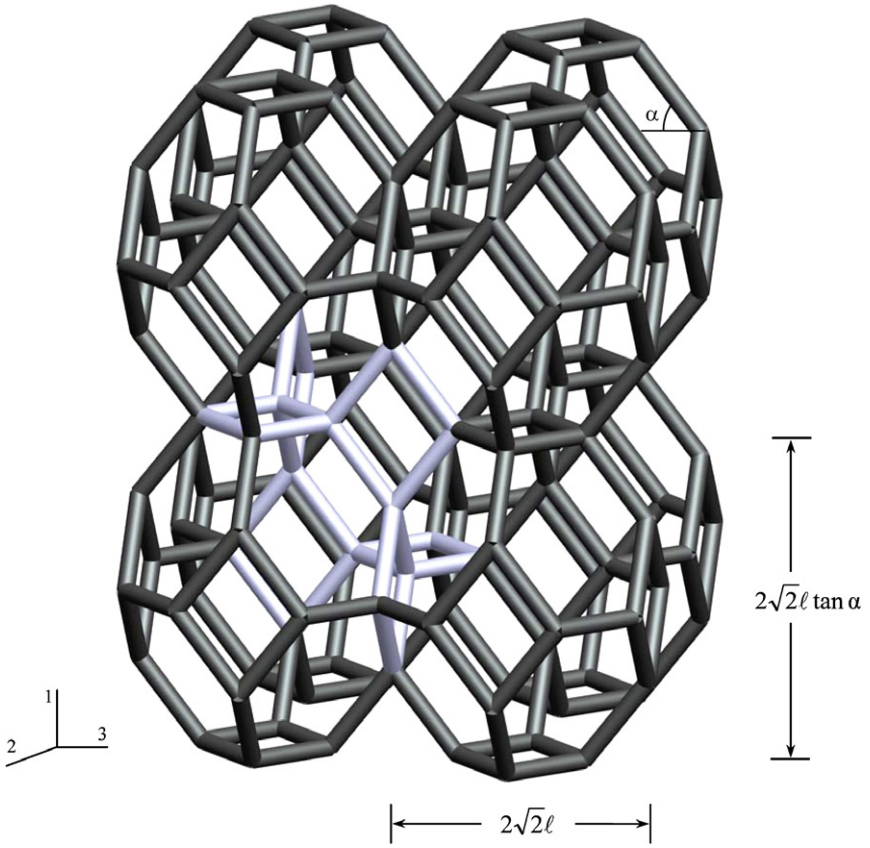

Fig. 20. Cluster of anisotropic Kelvin cells.

4. Modeling of solid foams

The PU and Al foams will be modeled first by adopting the perfectly ordered structure, based on Kelvin's 14-sided cell also used by GKJ (see Thompson, 1887 and literature review in GKJ). We also consider a cluster of Kelvin cells with randomly perturbed vertices creating an irregular foam. The most realistic models considered involve disordered foams generated with the Surface Evolver. The ligaments in the three types of models are represented as shear deformable beams whose geometry is based on the area distributions measured in the PU and Al foams in Section 2. Anisotropy is introduced to the models using a consistent scheme that results in cell elongation in the rise direction. The geometric characteristics of the model foams will now be described.

4.1. Ligament geometry

The ligaments are assumed to be straight with length ℓ but different cross sectional geometries and area distributions are used for the PU and Al foams. The PU ligaments have the same three-cusp hypocycloid cross section of radius r adopted in GKJ (see Fig. 21). The cross sectional area varies along the length according to Eq. (1) with the constants $c_1 = 96$ and $c_2 = 1$. The area and moments of inertia of this section are given by

$$A = \left(\sqrt{3} - \frac{\pi}{2}\right) r^2, \qquad I_y = I_z = \frac{1}{24}(20\sqrt{3} - 11\pi) r^4, \qquad J = 0.0021 r^4. \tag{3}$$

(J due to Warren et al., 1997)

The volume of solid depends on ligament length ℓ and the mid-span radius r_o. These parameters appear in the elastic moduli through their ratio r_o/ℓ. The value of r_o depends on the relative density through the calibrated relationships given in Section 4.3.

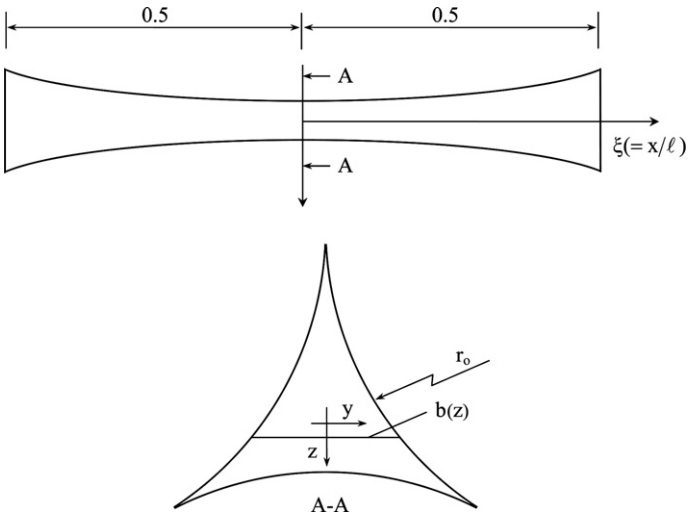

Fig. 21. Definition of geometry of PU foam ligaments.

The Al ligament cross sections were idealized as equilateral triangles or as circles (see also Schmierer and Razani (2006) who have proposed a couple of alternative cross sections that are between a circle and a triangle). The triangular section has the following geometric parameters (a is the length of the triangle sides-Fig. 22):

$$A = \frac{\sqrt{3}}{4}a^2, \qquad I_y = I_z = \frac{\sqrt{3}}{96}a^4, \qquad J = \frac{\sqrt{3}}{80}a^4. \tag{4a}$$

The corresponding parameters for the circular section (radius R) are

$$A = \pi R^2, \qquad I_y = I_z = \frac{\pi R^4}{4}, \qquad J = \frac{\pi R^4}{2}. \tag{4b}$$

In both cases the cross sectional area varies along the length according to Eq. (1) with $c_1 = 36$ and $c_2 = 1$.

4.2. Anisotropy

Anisotropy is introduced to the Kelvin and random foams through the procedure of GKJ. All ligaments with a projection in the x_1-direction are elongated so that this projection is amplified by the factor λ while the projections in the x_2- and x_3-directions retain their original lengths. Thus, for example, the Kelvin cell height becomes $h_1 = 2\sqrt{2}\ell \tan\alpha$ while the width remains $h_2 = 2\sqrt{2}\ell$, where

$$\frac{h_1}{h_2} = \tan\alpha = \lambda \tag{5}$$

as shown in Fig. 20 (Dement'ev and Tarakanov (1970) used a similar geometric distortion of the Kelvin cell to represent anisotropy).

4.3. Correction for the volume of material in the nodes

When ligaments are modeled as beams that connect four to each node, the ends of the beams overlap. It is important to account for excess material when calculating the material volume. GKJ removed the excess material by cutting the ends of the beams with appropriately chosen smooth curved surfaces. Figs. 23–25 show nodes generated by this process for the Plateau border, triangular and circular ligament cross sections. For the first two the ligaments do not mate smoothly after removing material while the circular ligaments do.

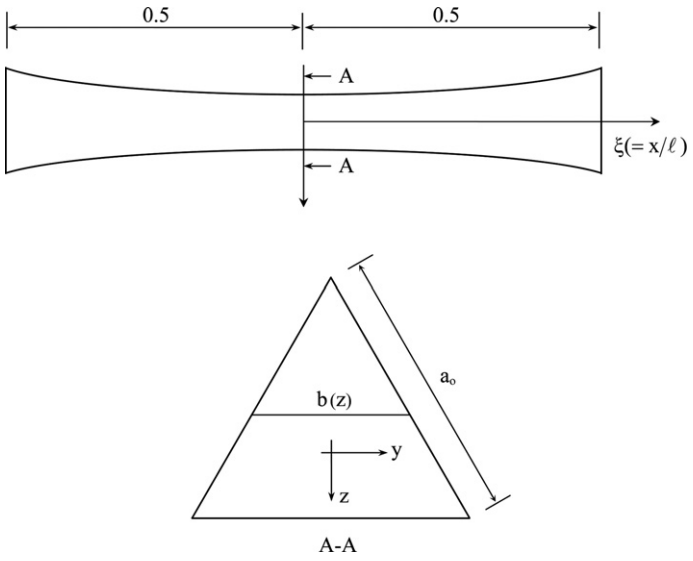

Fig. 22. Definition of geometry of Al foam ligaments.

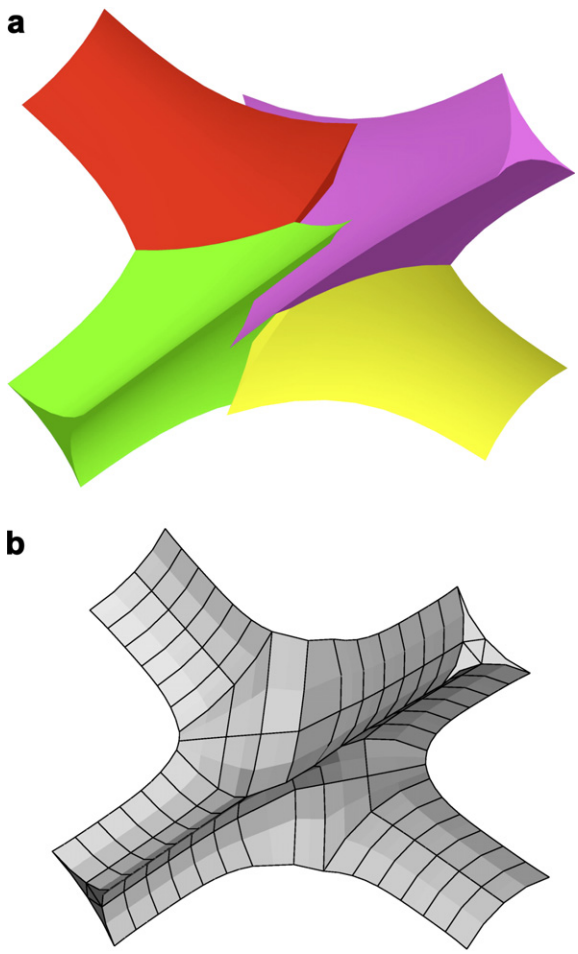

Fig. 23. (a) A Kelvin cell node for PU foam model consisting of four converging beam ligaments with intersecting material removed. (b) Same node as represented by solid FEs.

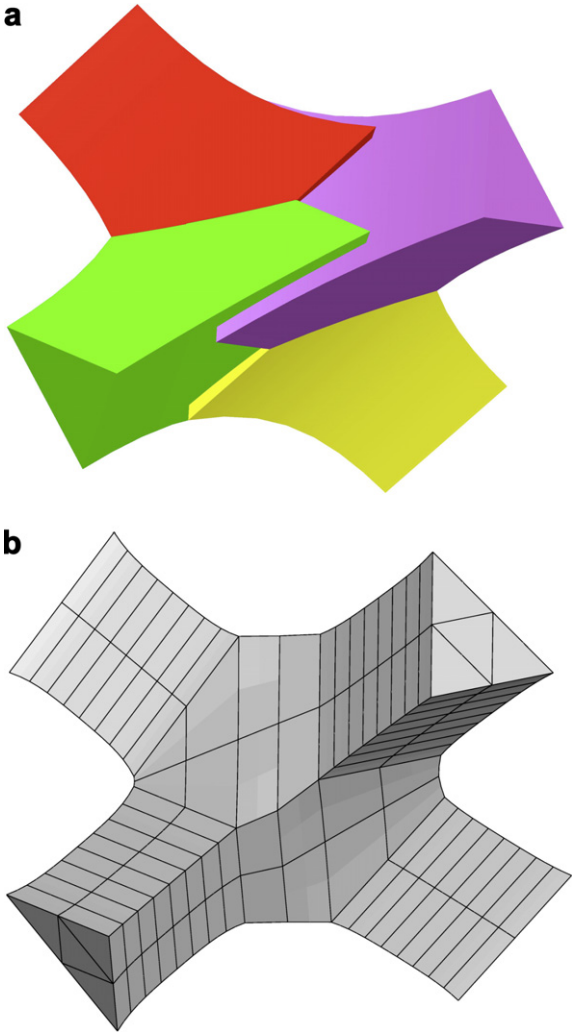

Fig. 24. (a) A Kelvin cell node for Al foam model consisting of four converging triangular cross section beam ligaments with intersecting material removed. (b) Same node as represented by solid FEs.

Without this correction, the relative density is proportional to the respective geometric ratios raised to the power of 2, i.e., $\{(r_o/\ell)^2, (a_o/\ell)^2, (R_o/\ell)^2\}$ where $\{r_o, a_o, R_o\}$ are the characteristic cross sectional dimensions at mid-span. With the correction, the power is no longer 2 and furthermore depends on the anisotropy according to the powerlaw relationship.

$$\frac{\rho^*}{\rho} = k\left(\frac{X_o}{\ell}\right)^n, \qquad X_o \in \{r_o, a_o, R_o\}. \tag{6}$$

Table 3 lists k and n for anisotropy values $1 \leqslant \lambda \leqslant 1.4$ for PU foams with the particular cross sectional area distribution given above (see also Fig. 6; note that the numbers differ slightly from the corresponding values in Table 3 of GKJ because of a small difference in their area distribution function).

Table 4 lists k and n for the two ligament cross sections for the Al foams with the area distribution function in Fig. 14.

We note that the material observed in closed faces of the Duocel foams is not accounted for in these calculations. Consequently the estimated ligament dimensions are somewhat larger than in the actual foam.

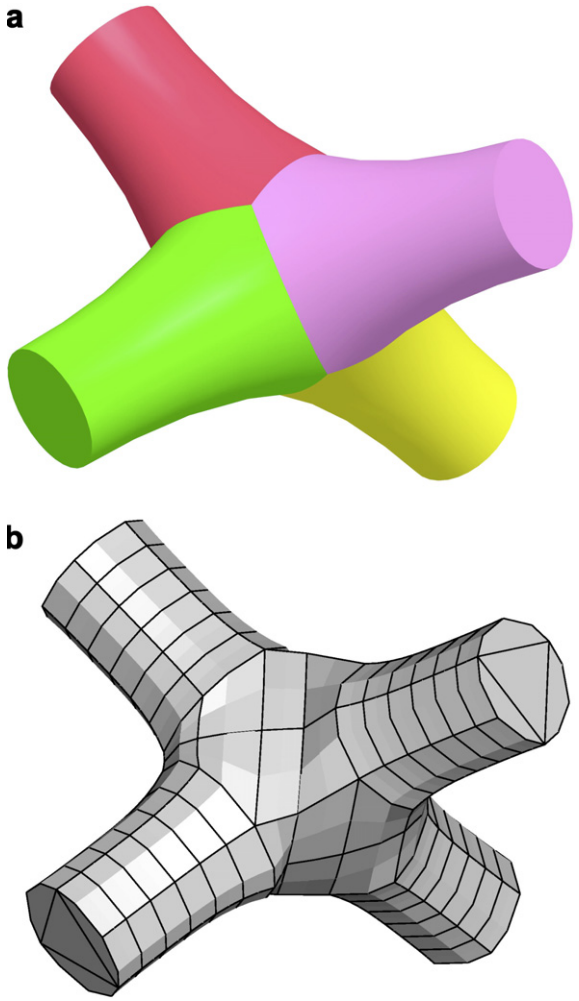

Fig. 25. (a) A Kelvin cell node for Al foam model consisting of four converging circular cross section beam ligaments with intersecting material removed. (b) Same node as represented by solid FEs.

Table 3
Fit parameters for correcting the relative density of PU foams with Eq. (6)

λ	n	k
1.00	1.6731	0.1677
1.10	1.6739	0.1596
1.20	1.6762	0.1535
1.30	1.6796	0.1488
1.40	1.6839	0.1453

4.4. Kelvin cell model

The Kelvin cell consists of 6 squares, 8 hexagons and 36 ligaments and fills the space; consequently its initial elastic response can be captured by limiting attention to a characteristic cell. GKJ created anisotropic microstructures as described in Section 4.2 and illustrated in Fig. 20. The corresponding characteristic cell is shown in Fig. 26. When the ligaments are modeled as beams the periodicity conditions of this cell are as follows: let the three pairs of opposite bounding faces of the cell be $(\partial R_{i1}, \partial R_{i2})$ $i = 1, 3$. The displacements and rotations

Table 4
Fit parameters for correcting the relative density of Al foams with Eq. (6)

λ	Circular		Triangular	
	n	k	n	k
1.00	1.7072	2.0263	1.4613	0.3014
1.10	1.7131	1.9543	1.4693	0.2912
1.20	1.7189	1.8985	1.4730	0.2823
1.30	1.7250	1.8561	1.4785	0.2762
1.40	1.7312	1.8231	1.4856	0.2720

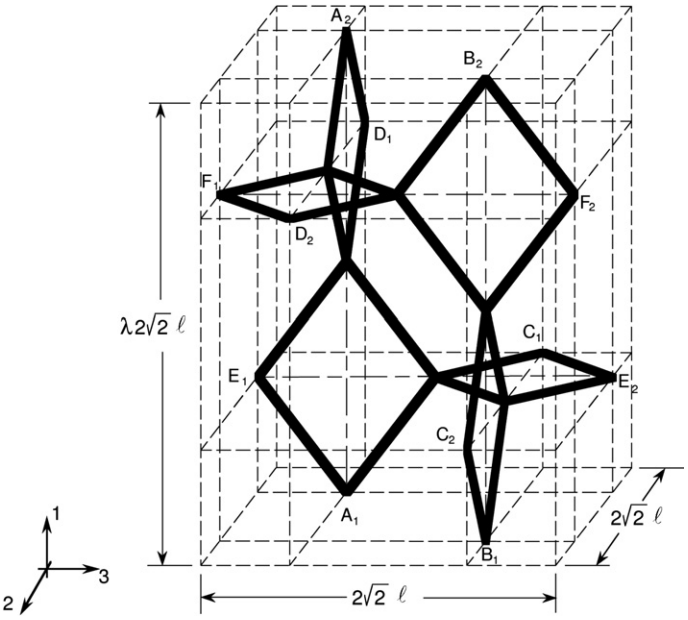

Fig. 26. The Kelvin foam characteristic cell.

of points on these faces are respectively denoted by (u_{i1}, u_{i2}) and $(\theta_{i1}, \theta_{i2})$ $i = 1, 3$. The following relationships for degrees of freedom are prescribed for points on each pair of faces $(\partial R_{i1}, \partial R_{i2})$ $i = 1, 3$

$$\begin{aligned} &u_{i1} - u_{i2} = u_{i1}^{\text{ref}} - u_{i2}^{\text{ref}}, \quad i = 1, 3, \\ &\theta_{i1} - \theta_{i2} = 0, \quad i = 1, 3, \end{aligned} \tag{7}$$

where u_{ij}^{ref} are displacements of conjugate points on opposite sides chosen as reference points (e.g., (A_1, A_2), (C_1, C_2), etc.).

In this model the mid-span variables $\{r_o, a_o, R_o\}$ were evaluated from Eq. (6) based on the ligament length of the initial isotropic Kelvin cell. The fact that the anisotropic versions have ligaments of two different lengths was not accounted for.

4.5. Irregular "Kelvin" cell model

An irregular anisotropic foam is generated by perturbing the coordinates of the nodes of the Kelvin cells. This preserves the number of faces but makes them irregular polygons. (For alternative methods of generating a random foam based on the Voronoi scheme, see for example, Zhu et al., 2000; Roberts and Garboczi, 2002; Gan et al., 2005; Kraynik et al., 2003). We start with a domain of $N \times N \times N$ Kelvin cells with anisotropy of λ

and perturb the nodes as follows. Let $\boldsymbol{x}_o$ represent the initial position vector of a node in the anisotropic Kelvin cell. The position vector in the perturbed configuration, x, is given by

$$\boldsymbol{x} = \boldsymbol{x}_o + p\boldsymbol{\xi}\ell, \qquad 0 \leqslant \boldsymbol{\xi}_i \leqslant 0.5, \quad i = 1,3, \tag{8}$$

where ξ_i are the amplitudes of the disturbance and p is a normally distributed random number between -0.5 and 0.5. The perturbed nodes retain the connectivity of the Kelvin model. The disturbance applied to the nodes on opposite faces of the $N \times N \times N$ cell domain is chosen so as to accommodate periodic boundary conditions. The domain is then analyzed with full periodicity. Fig. 27 compares five cells in an anisotropic foam with $\lambda = 1.2$ (a) and the same cells after distortion with amplitude $\xi_i = 0.3$ ($i = 1,3$) was applied (b) (0.3 was chosen as it results in realistic cell geometries).

The mid-span variables $\{r_o, a_o, R_o\}$ are evaluated from Eq. (6) using the ligament length of the initial isotropic Kelvin cell and the chosen anisotropy. The measurements performed on both the PU and Al foams clearly show that A_o depends on ℓ. This effect was introduced in the following approximate manner. The average length of all ligaments ($\bar{\ell}$) in the perturbed model was calculated. The lengths were then grouped into two categories, those longer and those shorter than $\bar{\ell}$, and the average length of each category ($\bar{\ell}_1, \bar{\ell}_2$) was established. The two average lengths were then used in the appropriate version of Eq. (2) (PU and Al versions) to establish values for A_o. The effect of this change on the foam density, if any, was not considered.

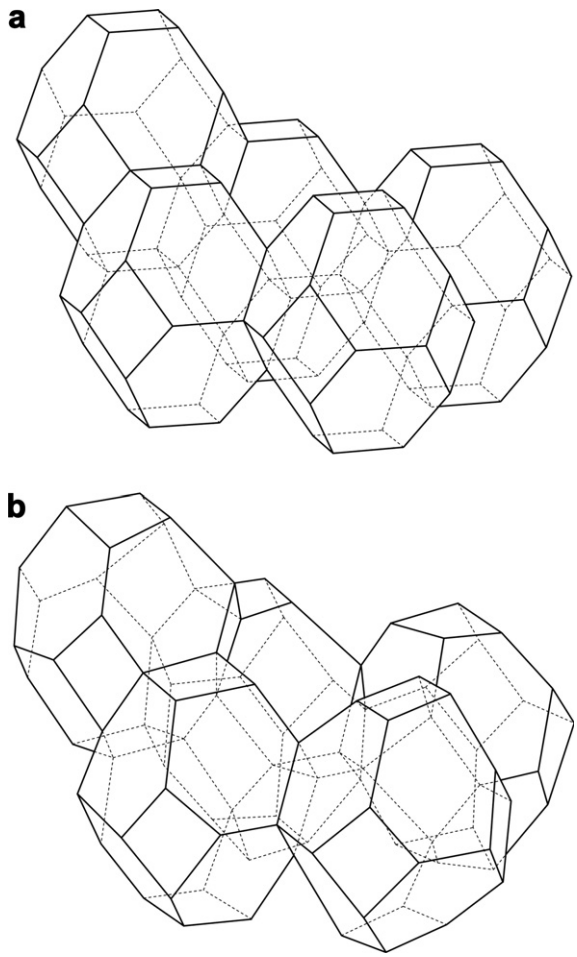

Fig. 27. (a) Five cells of an anisotropic Kelvin cell foam with $\lambda = 1.20$. (b) Same cells after perturbation with amplitude $\xi_i = 0.3$ ($i = 1,3$) was applied.

4.6. Random foam

The nodes of a spatially periodic random foam with N^3 cells are calculated with the Surface Evolver. The nodal coordinates are then displaced to obtain the desired anisotropy as described in Section 4.2. The relative density is determined by relating $\{r_o, a_o, R_o\}$ to the average length, $\bar{\ell}$, according to the powerlaw relationship (6) for specified values of λ. The scheme described in Section 4.5 was used to generate two values of A_o based on the ligament length. Once again, any effect this may have had on the relative density was neglected.

4.7. Discretization

The ligaments are discretized with finite elements within the nonlinear code ABAQUS using the B32, 3-node quadratic space beam element. Each ligament is represented by 8 elements of uniform cross sectional area. The area of each element is listed in Table 5. The values are based on the symmetric function $f(\xi)$ in (1) using the appropriate calibration constants for PU and Al. For the Kelvin cell model A_o in (1) is evaluated directly from (6) for selected values of relative density and anisotropy. For the irregular Kelvin and random foam models A_o depends on the ligament length as described in Section 4.5.

The Plateau border cross section of the PU foam is modeled by using the *beam general section* feature of ABAQUS. The beam elements are made to be shear-deformable by including the strain energy due to transverse shear as follows:

$$U_s = \int_{-1/2}^{1/2} \beta \frac{V^2(\xi)}{2GA} \ell \, \mathrm{d}\xi \quad \text{where } \beta = \frac{A}{I_z^2} \int_z \frac{Q^2(z)}{b(z)} \, \mathrm{d}z. \tag{9}$$

The second integral is over the cross section of the ligament shown in Figs. 21 and 22 with Q being the first moment of area about the y-axis ($b(z) \equiv$ width). For the Plateau border cross section shown in Fig. 21 $\beta = 1.24$. The triangular and circular beam cross sections used for the Al foam are available in the ABAQUS beam cross section library with $\beta = 6/5$ for equilateral triangles and $\beta = 10/9$ for circles.

The Kelvin characteristic cell models were also discretized with solid elements using C3D15V prisms for the ligaments and C3D27 brick elements for the nodes; full integration was chosen for both. The philosophy behind generating the mesh was to closely match the geometry of ligaments and nodes measured in our two families of foams. The main parts of the ligaments were assigned the area shapes and distributions represented by the appropriate functions $f(\xi)$ and were discretized with up to 32 prisms. The nodes were shaped with appropriate quadratic functions that approximate the geometry in the actual foams (see Figs. 23–25). The four ends of a node have the same shape as the ligaments that connect to them. The nodes are discretized with up to 24 brick elements. For the solid elements the material volume is easily calculated by summing the volume of all elements. Since the actual PU and Al foams analyzed had relative densities of about 2.5% and 7.5%, these are the only two densities for which solid model calculations will be performed. This discretization results in approximately 24,000 degrees of freedom and Lagrange multipliers making this model an order of magnitude larger than the corresponding beam model. This level of computational effort was prohibitively expensive for the much larger number of cells in the other two models and consequently they were discretized with only beam elements.

Table 5
Cross sectional area of uniform beam elements in the PU and Al ligaments

	$f(\xi)$ PU	$f(\xi)$ Al
$0 \leqslant \lvert\xi\rvert \leqslant 0.2$	1	1
$0.2 < \lvert\xi\rvert \leqslant 0.3$	1.544	1.172
$0.3 < \lvert\xi\rvert \leqslant 0.4$	2.799	1.663
$0.4 < \lvert\xi\rvert \leqslant 0.5$	5.705	3.227

5. Elastic moduli results

The various models developed were used to predict the moduli of the two classes of materials and to perform limited parametric studies. The predictions will include those based on closed form expressions for the anisotropic Kelvin cell developed in GKJ using Eqs. (1) and (6) for $A(\xi)$ and the appropriate density ratios (see Table 4 of GKJ). In these analyses the ligaments were modeled as shear deformable, extensional beams and consequently the results are usually in very good agreement with the numerical characteristic cell beam model described in Section 4.4.

5.1. Polyester urethane foams

We start by predicting the elastic moduli in the rise (E_1^*) and the transverse directions (E_2^*) for the five PU foams in Table 1. Predictions from the analytic expressions, the Kelvin cell model, the irregular Kelvin model, from the random model and from the Kelvin cell modeled with solid elements are listed in Table 6. Included in the Table are the measured moduli in the two directions. As in GKJ, the solid element Kelvin cell model gives the highest moduli in both directions. These results are also generally the closest to the experimental values with absolute differences for E_1^* ranging from 5% to 25%. As expected, the predictions from the analytical and numerical Kelvin cell models are close to each other and somewhat lower than the solid model values; the difference from the experimental values for E_1^* ranges from 4% to 32%. Interestingly, the random model is somewhat stiffer than the Kelvin models but only by 3–6%. The irregular Kelvin cell model gives the lowest moduli in both directions and consequently is the furthest from the experimental results. (Note that the last predictions are averages of ten calculations as this number was found to result in converged mean values. Increasing the parameter ξ_i increases the standard deviation of the predictions but the mean values are relatively insensitive to this parameter.)

Many foam property calculations are based on a perfectly ordered structure with the ligaments modeled as uniform cross section beams. It is thus interesting to consider simpler versions of the Kelvin cell model in which the anisotropy and correction for material at the nodes are neglected and the ligaments are modeled as Bernoulli–Euler beams of uniform cross section. Results for such models appear in the literature (e.g., Warren and Kraynik, 1997; Zhu et al., 1997; Laroussi et al., 2002) and can also be deduced from the formulas in Table 4 of GKJ. The axial moduli calculated in this manner for our five PU foams for circular (C) and Plateau

Table 6
Comparison of calculated and measured moduli for PU foams

	3 ppi	10 ppi	20 ppi	45 ppi	100 ppi
ρ^*/ρ (%)	2.18	2.47	2.36	2.44	2.82
λ	1.423	1.342	1.276	1.247	1.211
E_1^*/E (%)	**0.227**	**0.181**	**0.200**	**0.215**	**0.229**
Analytic	0.155	0.188	0.158	0.163	0.215
Kelvin cell	0.156	0.189	0.159	0.164	0.215
Kelvin pert.[a]	0.135	0.169	0.140	0.146	0.191
Random	0.166	0.200	0.167	0.173	0.225
Solid	0.169	0.205	0.174	0.181	0.240
E_2^*/E (%)	**0.070**	**0.071**	**0.119**	**0.103**	**0.128**
Analytic	0.055	0.078	0.078	0.088	0.120
Kelvin cell	0.055	0.078	0.079	0.088	0.119
Kelvin pert.[a]	0.050	0.074	0.073	0.080	0.111
Random	0.057	0.081	0.081	0.089	0.123
Solid	0.060	0.085	0.086	0.095	0.134
Basic Kelvin Analysis-C[b]	0.0280	0.0358	0.0327	0.0350	0.0465
Basic Kelvin Analysis-PB[b]	0.0464	0.0594	0.0543	0.0579	0.0770

[a] Perturbation $\xi_i = 0.3$; model size $8 \times 8 \times 8$ cells; values are average of 10 calculations.
[b] E^*/E (%) values. $E = 10$ ksi (69 MPa), $\nu = 0.49$ (GKJ).

border (PB) cross section ligaments are listed in Table 6 under "Basic Kelvin". In concert with the observations of GKJ, both sets of predictions are unrealistically low. The predictions for circular ligaments are lower than the experimental values of E_1^*/E by factors of 5–8 and for Plateau border ligaments by factors of 3–5.

We now use the various models to conduct a limited parametric study of foam moduli. Fig. 28a shows predictions of E_1^* and E_2^* as a function of the anisotropy parameter λ for foams of relative density of 2.5% (numerical results are listed in Table 7). The two moduli vary essentially linearly with anisotropy for all models, with E_1^* increasing and E_2^* decreasing with λ. The solid element Kelvin cell model yields the highest values with the random and Kelvin cell beam models somewhat lower. The differences between the random and Kelvin cell models is about 5–10% for E_1^* and less for E_2^*. The irregular Kelvin cell model has the lowest moduli.

Fig. 28b shows predictions of both moduli as a function of relative density for $\lambda = 1.3$ (numerical results are listed in Table 8). We expect the material distribution in the ligaments and the nodes to vary to some degree with relative density. Since our geometric information originated from foams with ρ^*/ρ in the range of 2.2–2.8%, extrapolation to much higher and much lower densities may not be valid and for this reason we limit our calculations to $0.1\% \leqslant \rho^*/\rho \leqslant 4\%$. For the same reason it was not possible to construct solid element

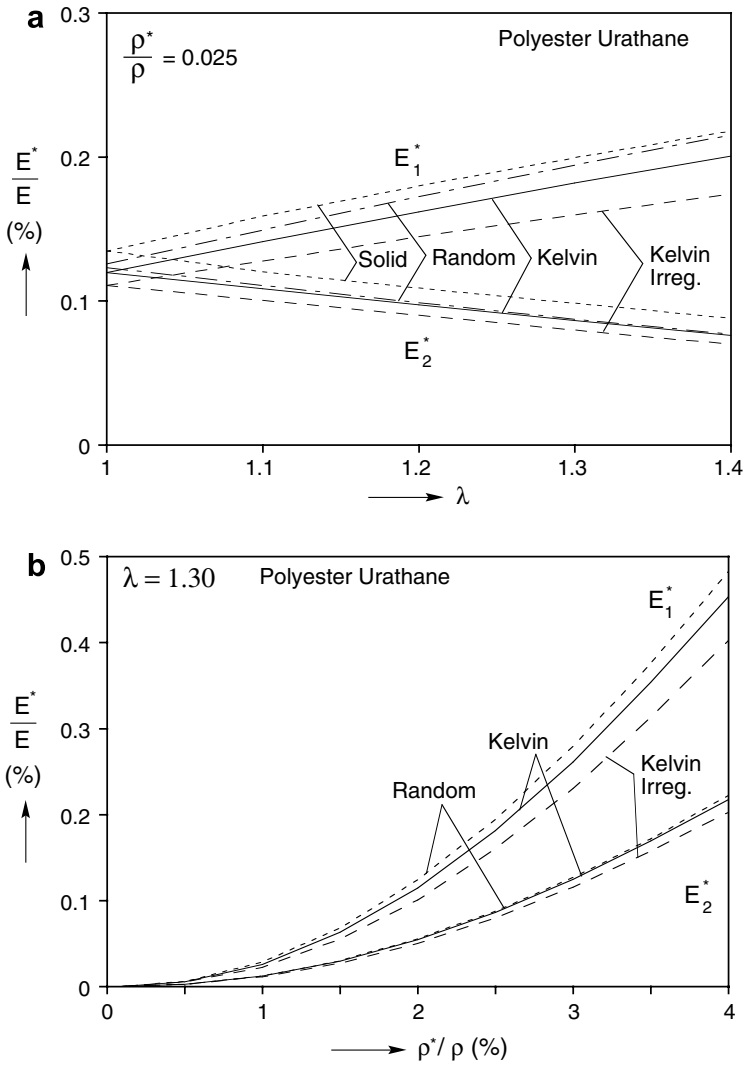

Fig. 28. (a) Predicted elastic moduli as a function of anisotropy for PU foams. (b) Predicted elastic moduli as a function of relative density for PU foams.

Table 7
Elastic moduli for PU foams of different anisotropy values and $\rho^*/\rho = 2.5\%$

λ	E_1^*/E (%)				
	Analytic	Kelvin cell	Kelvin perturbed[a]	Random	Solid
1.0	0.1194	0.1196	0.1106	0.1256	0.1344
1.1	0.1406	0.1410	0.1278	0.1492	0.1589
1.2	0.1612	0.1619	0.1445	0.1724	0.1798
1.3	0.1808	0.1819	0.1599	0.1942	0.1994
1.4	0.1992	0.2007	0.1741	0.2150	0.2176
λ	E_2^*/E (%)				
	Analytic	Kelvin cell	Kelvin perturbed[a]	Random	Solid
1.0	0.1194	0.1196	0.1106	0.1230	0.1344
1.1	0.1083	0.1085	0.1004	0.1107	0.1201
1.2	0.0970	0.0972	0.0901	0.0988	0.1090
1.3	0.0861	0.0863	0.0798	0.0872	0.0983
1.4	0.0759	0.0762	0.0700	0.0768	0.0882

[a] Perturbation $\xi_i = 0.3$; model size $8 \times 8 \times 8$ cells; values are average of 10 calculations.

Table 8
Elastic moduli for PU foams of various relative density ratios and $\lambda = 1.30$

ρ^*/ρ (%)	E_1^*/E (%)			
	Analytic	Kelvin cell	Kelvin perturbed[a]	Random
0.10	1.17×10^{-4}	1.22×10^{-4}	1.12×10^{-4}	1.35×10^{-4}
1.00	0.0248	0.0255	0.0222	0.0280
2.00	0.1132	0.1146	0.1004	0.1237
3.00	0.2609	0.2608	0.2302	0.2791
4.00	0.4576	0.4529	0.4022	0.4825
ρ^*/ρ (%)	E_2^*/E (%)			
	Analytic	Kelvin cell	Kelvin perturbed[a]	Random
0.10	5.41×10^{-5}	5.64×10^{-5}	5.54×10^{-5}	5.75×10^{-5}
1.00	0.0116	0.0119	0.0109	0.0122
2.00	0.0536	0.0542	0.0499	0.0551
3.00	0.1248	0.1243	0.1151	0.1266
4.00	0.2206	0.2172	0.2022	0.2221

[a] Perturbation $\xi_i = 0.3$; model size $8 \times 8 \times 8$ cells; values are average of 10 calculations.

Kelvin cell models and thus results from only the three beam models are presented. The predictions follow the powerlaw dependence on relative density implied by the closed form expression in Table 4 of GKJ (exponent >2). The random foams have somewhat higher moduli than the Kelvin cell foams while the irregular Kelvin foams have the lowest. For example, for ρ^*/ρ of both 2% and 4% the Kelvin cell predictions for E_1^* are approximately 9% lower than the random foam.

5.2. Aluminum foams

Predictions for the Al foams are compared to measurements in Table 9. Note that each measurement corresponds to foam specimens of different densities because of the small density variations through the original foam blocks. In general the predictions for both directions are somewhat higher than the measurements. The values for the triangular ligaments were somewhat higher than those from the circular ones mainly because of different amount of material in the nodes (see analytic predictions from the two models in Table 9). The numerical results quoted originate from the circular ligaments. Interestingly, the highest predictions come

Table 9
Comparison of calculated and measured moduli for Al foams

	10 ppi	20 ppi	40 ppi
λ	1.27	1.24	1.18
ρ^*/ρ(%)	8.63	8.37	8.20
E_1^*/E(%)	**0.863**	**0.857**	**0.780**
Analytic-C	1.067	0.975	0.875
Analytic-T	1.170	1.063	0.950
Kelvin cell	1.068	0.977	0.876
Kelvin pert.[a]	0.973	0.886	0.797
Random	1.131	1.033	0.930
Solid	1.271	1.155	1.039
ρ^*/ρ (%)	8.74	7.36	8.22
E_2^*/E (%)	**0.527**	**0.459**	**0.570**
Analytic-C	0.567	0.423	0.560
Analytic-T	0.624	0.447	0.609
Kelvin cell	0.568	0.423	0.560
Kelvin pert.[a]	0.529	0.394	0.522
Random	0.629	0.472	0.618
Solid	0.662	0.506	0.652

[a] Perturbation $\xi_i = 0.3$; model size $8 \times 8 \times 8$ cells; values are average of 10 calculations; $E = 10^4$ ksi (69 GPa), $v = 0.3$.

from the solid element Kelvin cell model, which is expected to have the best representation for the ligament stiffness and for the node geometry and stiffness. By not accounting for the material in the closed faces, the ligaments and therefore the foams are stiffer. Predictions from the analytic expressions and the Kelvin cell numerical model are again in very good agreement. The values are 3–24% higher than the measurements for E_1^* and −2% to 9% different for E_2^*. The random foam predictions are 10–31% higher for E_1^* and 8–22% higher for E_2^*. The predictions for the irregular Kelvin cell model are the closest to the experiments.

A more general comparison of measured and calculated moduli is shown in Fig. 29 where three experimental data points for each foam are plotted as a function of density. Included are predictions from the random and Kelvin cell foams using an average anisotropy of $\lambda = 1.2$. In the case of E_1^* (Fig. 29a) both models overpredict the data by 10–20% and the random foam is higher than the Kelvin cell model. The comparison between measurements and predictions is more favorable for E_2^* (Fig. 29b) and the predictions for both models are closer together.

Results from a limited parametric study of moduli are shown in Fig. 30. Fig. 30a shows predictions of E_1^* and E_2^* as a function of λ for foams of relative density of 7.5% (numerical results are listed in Table 10). Once again both moduli vary essentially linearly with anisotropy: E_1^* increases and E_2^* decreases with λ. The solid element Kelvin cell model is stiffer than the random and Kelvin cell beam models. The difference between the random and Kelvin cell models is about 5–10% for E_1^* and less for E_2^*. The irregular Kelvin cell model is the softest.

Fig. 30b shows predictions for the three models for both moduli as a function of density for $\lambda = 1.2$ (numerical results are listed in Table 11). Our information on material distribution in the ligaments and the nodes originated from foams with ρ^*/ρ in the range of 7.4–8.8% and consequently we limit our calculations to $6\% \leqslant \rho^*/\rho \leqslant 9\%$. Once more, it was not possible to construct solid element Kelvin cell models and thus the results from only the three beam models are presented. The predictions follow the powerlaw dependence on density implied by the closed form expression in Table 4 of GKJ (exponent not 2). The random foams is the stiffest and the irregular Kelvin model is the softest. For example, for ρ^*/ρ of both 6% and 9% the Kelvin cell predictions for E_1^* are approximately 6% lower than the random foam.

6. Summary and conclusions

Gong et al. (2005) demonstrated that open-cell foam microstructural characteristics such as the material distribution in the ligaments and nodes, and cell anisotropy play a decisive role in the mechanical behavior

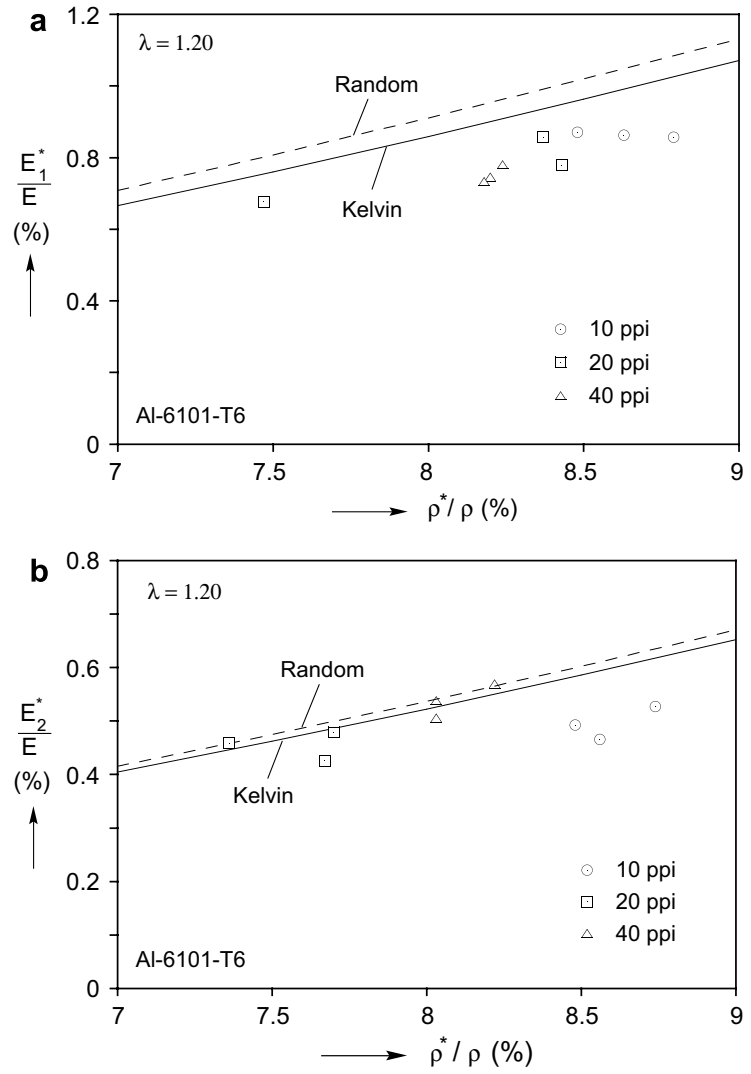

Fig. 29. Comparison of measured and calculated moduli for Al foams. (a) E_1^*/E and E_2^*/E.

of polymeric foams. In the present study micro-computed X-ray tomography was used to develop a more systematic data base on the microstructure of two classes of open-cell foams: polyester urethane and Duocel Al foams of various cell sizes. The PU foams had relative densities in the range of 2.2–2.8% and the Al foams in the range of 7.4–8.8%. Micro-CT generated 3D images were used to establish the cell anisotropy, the ligament length distribution, the cross sectional area along the length of the ligaments and other geometric characteristics. Both foams had similar random polyhedral cell microstructure and the cell size distribution was quite uniform. Both foams also exhibited anisotropy with λ ranging between 1.42–1.21 for PU and 1.27–1.18 for Al. The PU foam ligaments had the concave Plateau border cross sections characteristic of liquid foams, while the Al foams had rounded convex cross sections. In both cases the nodes contained a significant amount of material and typically, but not always, had four-way ligament connectivity. The PU nodes had smooth concave surfaces while those of the Al foam had rounder convex surfaces.

The measured geometric characteristics were used to build three spatially periodic FE foam models of increasing complexity. The first model is a perfectly ordered foam containing Kelvin cells. The second model consists of $N \times N \times N$ irregular Kelvin cells made by randomly perturbing the nodes. The third model represents a realistic random foam; it contains N^3 cells and is simulated with the Surface Evolver software. The cells

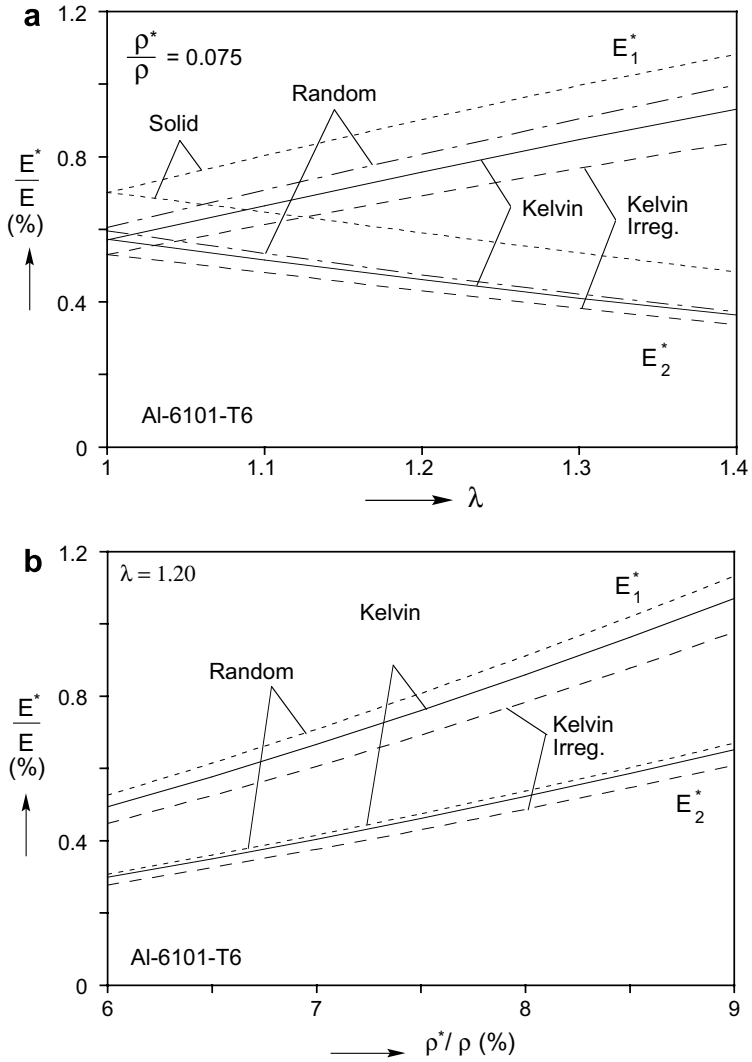

Fig. 30. (a) Predicted elastic moduli as a function of anisotropy for Al foams. (b) Predicted elastic moduli as a function of relative density for Al foams.

in all models the cells are elongated in one direction; the ligaments are assumed to be straight, to have non-uniform cross sectional area along the length. The ligaments in the PU foams have Plateau-border cross sections and those in the Al foams have circular or triangular cross sections. While solid elements provide the most accurate way to discretize these microstructures, the calculations would be prohibitively large for domains consisting of many cells. Consequently, solid elements were only practical for the model containing one characteristic Kelvin cell. The ligaments in all models were discretized as shear deformable beams instead. This approximation requires a correction when calculating the volume of solid because of the extra material in the nodes where beams intersect.

The performance of the three models was then evaluated by comparing predictions for the foam elastic moduli with measurements on the PU and Al foams. The models were also used to conduct parametric studies on foam density and anisotropy. The results support the following observations:

- The Kelvin cell and the random foam models predicted the measured moduli very well for the PU foams but gave somewhat higher values for the Al foams. The random foam predictions were 5–10% higher than the Kelvin foam.

Table 10
Elastic moduli for Al foams of different anisotropy values and $\rho^*/\rho = 7.5\%$

λ	E_1^*/E (%)						
	Solid model		Beam model				
	Solid-C	Solid-T	Analytic-C	Analytic-T	Kelvin cell	Kelvin perturbed[a]	Random
1.0	0.7007	0.7517	0.5701	0.6038	0.5720	0.5304	0.6044
1.1	0.8033	0.8610	0.6648	0.7066	0.6670	0.6128	0.7079
1.2	0.9018	0.9683	0.7572	0.8058	0.7598	0.6920	0.8068
1.3	0.9955	1.0672	0.8461	0.8969	0.8492	0.7672	0.9046
1.4	1.0817	1.1598	0.9310	0.9804	0.9346	0.8384	0.9988
λ	E_2^*/E (%)						
	Solid model		Beam model				
	Solid-C	Solid-T	Analytic-C	Analytic-T	Kelvin cell	Kelvin perturbed[a]	Random
1.0	0.7007	0.7517	0.5701	0.6038	0.5720	0.5304	0.5951
1.1	0.6476	0.6947	0.5141	0.5465	0.5158	0.4799	0.5338
1.2	0.5896	0.6343	0.4597	0.4895	0.4613	0.4297	0.4744
1.3	0.5344	0.5744	0.4086	0.4336	0.4100	0.3818	0.4211
1.4	0.4816	0.5179	0.3616	0.3816	0.3630	0.3374	0.3731

[a] Perturbation $\xi_i = 0.3$; model size $8 \times 8 \times 8$ cells; values are average of 10 calculations.

Table 11
Elastic moduli for Al foams of various density ratios and $\lambda = 1.20$

ρ^*/ρ (%)	E_1^*/E (%)				
	Analytic-C	Analytic-T	Kelvin cell	Kelvin perturbed[a]	Random
6.0	0.4910	0.4926	0.4933	0.4476	0.5264
6.5	0.5746	0.5892	0.5771	0.5242	0.6146
7.0	0.6635	0.6937	0.6661	0.6057	0.7081
7.5	0.7575	0.8058	0.7602	0.6920	0.8068
8.0	0.8559	0.9253	0.8587	0.7827	0.9105
8.5	0.9595	1.0518	0.9623	0.8777	1.0188
9.0	1.0672	1.1851	1.0699	0.9767	1.1315
ρ^*/ρ (%)	E_2^*/E (%)				
	Analytic-C	Analytic-T	Kelvin cell	Kelvin perturbed[a]	Random
6.0	0.2969	0.2979	0.2983	0.2770	0.3071
6.5	0.3480	0.3568	0.3494	0.3248	0.3595
7.0	0.4024	0.4207	0.4039	0.3757	0.4153
7.5	0.4599	0.4895	0.4615	0.4297	0.4744
8.0	0.5203	0.5628	0.5219	0.4865	0.5366
8.5	0.5840	0.6405	0.5856	0.5461	0.6018
9.0	0.6502	0.7226	0.6518	0.6083	0.6699

[a] Perturbation $\xi_i = 0.3$; model size $8 \times 8 \times 8$ cells; values are average of 10 calculations.

- For both materials the Kelvin cell model with solid elements gave the highest moduli and the irregular Kelvin model the lowest.
- The Al foams analyzed contained randomly dispersed closed cell faces that were not accounted for in the models, resulting in somewhat higher ligament volume than the actual foams. This has the effect of increasing the predicted moduli.

The results clearly indicate that modeling foam ligaments as shear deformable beams is effective and efficient provided key geometric characteristics of real foams are incorporated into the analysis. These include cell anisotropy, nonuniform area distribution along the ligaments and correction for the material in the nodes.

If these features are not properly represented but the ligaments are modeled as Bernoulli–Euler beams with uniform cross sections, the moduli can be off by nearly an order of magnitude.

Finally, real foams have a random microstructure so random foam models generated with the Surface Evolver are undoubtedly the most realistic. The symmetry and perfect order of the Kelvin microstructure is clearly an oversimplification. Despite this, the elastic moduli predicted by the Kelvin cell models are within engineering accuracy of predictions for random foams. In view of the numerical efficiency of the Kelvin cell model, it is clearly a very effective engineering tool for calculating elastic properties of foams. Whether this conclusion can be extended to inelastic properties of foams remains to be seen.

Acknowledgements

The work of W.Y.J. and S.K. was supported by National Science Foundation through Grant CMS-0527906. The work of A.M.K. was supported by Sandia National Laboratories. Sandia is a multiprogram laboratory operated by Sandia Corporation, a Lockheed Martin Company, for the United States Department of Energy's National Nuclear Security Administration under contract DE-AC04-94AL85000. Both sources of support are acknowledged with thanks. The authors wish to thank B.D. Leyda and E.R.G. for providing the Duocel aluminum foam samples used in the study at our specifications. Thanks are also due to Foamex International Inc. for providing the polymeric foam samples analyzed in this project. We are grateful to Scanco engineers for their support in multiple ways in the use of our micro-CT-80 system and to Robert Ketcham for his insightful tutorials on X-ray tomography. Finally we are thankful to Lixin Gong for his help in multiple ways in the course of this study.

Appendix A. Main specifications of *Scanco Medical AG* μCT 80

- Peak energy: 45/55/70 kVp.
- Current intensity: 57/114 μA.
- Strip detector: 50×6 mm with 1024×128 pixels (48 μm pitch).
- Resolution: 10–74 μm nominal isotropic.
- At maximum resolution 2000 projections per 360°.
- Maximum specimen size: 75.8 mm in diameter, 120 mm in height.
- For a 75.8 mm diameter specimen 100 slices are taken per 3.7 mm height (at maximum resolution).
- Scan time: $2k \times 2k$ 7–14 s/slice (12–25 min/108 slices).
- Reconstruction time: 48 s/slice for $2k \times 2k$, 0.18° angular increment.
- Data acquisition: HP AlphaStation single processor system with 1GB memory, 300 GB hard disk space, SDLT tape drive.
- For a $50 \times 50 \times 50$ mm specimen, maximum resolution, it takes about 48 h for scanning and reconstruction, yields around 40 GB data.

References

Ashby, M.F., Evans, A., Fleck, N.A., Gibson, L.J., Hutchinson, J.W., Wadley, H.N.G., 2000. Metal Foams: A Design Guide. Butterworth–Heinemann.

ASTM E 1441-00, 1992. Standard guide for computed tomography (CT) Imaging.

Benouali, A.-H., Froyen, L., Dillard, T., Forest, S., N'Guyen, F., 2005. Investigation on the influence of cell shape anisotropy on the mechanical performance of closed cell aluminium foams using micro-computed tomography. In: Mechanical Behavior of Cellular Solids. J. Mater. Sci. 40, 5801–5811.

Brakke, K.A., 1992. The surface evolver. Exp. Math. 1, 141–165. Available from: <http://www.susqu.edu/facstaff/b/brakke/evolver/>.

Dement'ev, A.G., Tarakanov, O.G., 1970. Model analysis of the cellular structure of plastic foams of the polyurethane type. Mekh. Polim. 5, 859–865, Translation pp. 744–749.

Gan, Y.X., Chen, C., Shen, Y.P., 2005. Three-dimensional modeling of the mechanical property of linearly elastic open cell foams. Int. J. Solids Struct. 42, 6628–6642.

Gibson, L.J., Ashby, M.F., 1997. Cellular Solids: Structure and Properties, second ed. Cambridge University Press.

Gong, L., Kyriakides, S., 2005. Compressive response of open cell foams. Part II: Initiation and evolution of crushing. Int. J. Solids Struct. 42, 1381–1399.

Gong, L., Kyriakides, S., Jang, W.-Y., 2005. Compressive response of open-cell foams. Part I: Morphology and elastic properties. Int. J. Solids Struct. 42, 1355–1379.

Hilyard, N.C., Cunningham, A. (Eds.), 1994. Low Density Cellular Plastics: Physical Basis of Behavior. Chapman & Hall, London.

Huber, A.T., Gibson, L.J., 1988. Anisotropy of foams. J. Mater. Sci. 23, 3031–3040.

Ketcham, R.A., Carlson, W.D., 2001. Acquisition, optimization and interpretation of X-ray computed tomographic imagery: applications to the geosciences. Comput. Geosci. 17, 381–400.

Kraynik, A.M., 2003. Foam structure: from soap froth to solid foams. MRS Bull. 28 (4), 275–278.

Kraynik, A.M., 2006. The structure of random foam. Adv. Eng. Mater. 8–9, 900–906.

Kraynik, A.M., Reinelt, D.A., van Swol, F., 2003. Structure of random monodisperse foam. Phys. Rev. E 67 (031403), 1–11.

Kraynik, A.M., Reinelt, D.A., van Swol, F., 2004. Structure of random foam. Phys. Rev. Lett. 93 (20), 2083011–2083014.

Kraynik, A.M., Reinelt, D.A., van Swol, F., 2005. Structure of random bidisperse foam. Colloids Surf. A 263, 11–17.

Laroussi, M., Sab, K., Alaoui, A., 2002. Foam mechanics: nonlinear response of an elastic 3D-periodic microstructure. Int. J. Solids Struct. 39, 3599–3623.

Matzke, E.B., 1946. The three-dimensional shape of bubbles in foam – an analysis of the role of surface forces in three-dimensional cell shape determination. Am. J. Botany 33, 58–80.

Mills, N.J., 2007. The high strain mechanical response of the wet Kelvin model for open-cell foams. Int. J. Solids Struct. 44, 51–65.

Montminy, M.D., Tannenbaum, A.R., Macosko, C.W., 2004. The 3D structure of real polymer foams. J. Colloid Interface Sci. 280, 202–211.

Plateau, J.A.F., 1873. In: Statique Expérimentale et Théorique des Liquides Soumis aux Seules Forces Moléculaires, vol. 2. Gauthier-Villars, Paris.

Roberts, A.P., Garboczi, E.J., 2002. Elastic properties of model random three-dimensional open-cell solids. J. Mech. Phys. Solids 50, 33–55.

Schmierer, E.N., Razani, A., 2006. Self-consistent open-celled metal foam model for thermal applications. ASME J. Heat Transfer 128, 1194–1203.

Thompson, W. (Lord Kelvin), 1887. On the division of space with minimal partitional area. Philos. Magazine 24(5th Series), 503–514.

Warren, W.E., Kraynik, A.M., 1997. Linear elastic behavior of a low-density Kelvin foam with open cells. ASME J. Appl. Mech. 64, 787–794.

Warren, W.E., Neilsen, M.K., Kraynik, A.M., 1997. Torsional rigidity of a plateau border. Mech. Res. Commun. 24, 667–672.

Weaire, D., Hutzler, S., 1999. The Physics of Foams. Oxford University Press, Oxford.

Zhou, J., Allameh, S., Soboyejo, W.O., 2005. Microscale testing of the strut in open cell aluminum foams. J. Mater. Sci. 40, 429–439.

Zhu, H.X., Knott, J.F., Mills, N.J., 1997. Analysis of the elastic properties of open-cell foams with tetrakaidecahedral cells. J. Mech. Phys. Solids 45, 319–343.

Zhu, H.X., Hobdell, J.R., Windle, A.H., 2000. Effects of cell irregularity on the elastic properties of open-cell foams. Acta Mater. 48, 4893–4900.